NUMERICAL INVESTIGATION OF THE HYDRODYNAMIC FOCUSING PHENOMENA IN A MICROFLOW CYTOMETER

By

SAMUEL ARIEKELA

Bachelor of Engineering in Mechanical Engineering

Osmania University

Hyderabad, Andhra Pradesh

2007

Submitted to the Faculty of the
Graduate College of the
Oklahoma State University
in partial fulfillment of
the requirements for
the Degree of
MASTER OF SCIENCE
May, 2011

NUMERICAL INVESTIGATION OF THE HYDRODYNAMIC FOCUSING PHENOMENA IN A MICROFLOW CYTOMETER

Thesis Approved:

Dr. Khaled. A. Sallam

Thesis Adviser

Dr. Frank W. Chambers

Dr. Lorenzo Cremaschi

Dr. Mark E. Payton

Dean of the Graduate College

.

ACKNOWLEDGEMENTS

I would like to thank my adviser Dr.Khaled A.Sallam for his guidance and support throughout this project. I appreciate all his contributions of time and ideas.

I gratefully acknowledge my hearty appreciation to my advisory committee members Dr. Frank W. Chambers and Dr. Lorenzo Cremaschi.

I wish to thank my parents Pulmani and Anandam for raising me, supporting me and loving me. To them I dedicate my thesis. I thank my brother (Isaac), sister (Lavanya), sister-in-law (Tina) and my cute niece (Princy) for showing unconditional love towards me and strengthening me. I would like to thank my church family for their prayers and love and encouraging me throughout this project. I am grateful to my roommates, friends for helping me through difficult times and for all the entertainment and fun.

I thank almighty GOD for blessing me with strength and hope through his son Jesus Christ to complete this project.

TABLE OF CONTENTS

LIST OF FIGURES

LIST OF TABLES

NOMENCLATURE

l	Axial coordinate
a	Carreau model constant
$\overline{D}$	Deformation tensor
F_D	Drag force
n	Exponential index
d	Focused width of stream
r_1	Half width of the convergent part at starting location
r_2	Half width of the convergent part at the end
d/D	Hydrodynamic focusing ratio
L_m	Length at inversion point of convergent part
L_c	Length of convergent part
L_2	Length of outlet section
L_1	Length of sample inlet section
p	Pressure
r	Radial coordinate
Re	Reynolds number
Q_{sample}	Sample flow rate
u_s	Sample flow velocity

u_s	Sample flow velocity
$\dot{\gamma}$	Shear rate
$\overline{\tau}$	Shear stress tensor
u_{sh}	Sheath flow velocity
u_{sh}	Sheath flow velocity
T	Temperature
t	Time
Q_{Total}	Total flow rate
η_∞	Viscosity at infinite shear rate
η_0	Viscosity at zero shear rate
D_1,	Width of inlet channel 1
D_2	Width of inlet channel 2
D_3	Width of inlet channel 3

GREEK LETTERS

α	Volume fraction
ρ	Density
η	Non-Newtonian viscosity
μ	Dynamic viscosity
λ	Time relaxation constant

ABBREVIATIONS

CFD	Computational Fluid Dynamics
DEP	Dielectrophoretic
DPM	Discrete Phase Model

2-D	Two dimensional
UDF	User Defined Function
VR	Velocity ratio
VOF	Volume of Fluid

Chapter I

INTRODUCTION

1.1 Background

Flow cytometry is a technique to measure physical, chemical and functional properties of the biological particles which flow in a single file through a focused laser beam or a detector. A microfluidic device is used to guide the cells or microscopic particles in a single stream through a focused laser beam. The characteristic properties such as particle size, granularity, and complexity are studied using optics and electronics systems. This technique is widely used to count the cells and to study different characteristics of the cells, bacteria and microparticles. Flow cytometry is used extensively in the areas of disease diagnostics, immunology, genetics and applied in many research fields such as marine microbiology. The focus of this work is to investigate the hydrodynamic focusing phenomena of a micro flow cytometer.

1.1.1 Flow cytometer

A flow cytometer is made up of three main systems: fluidics, optics and electronics. The fluidics system guides the cells in a single file to the laser beam or the detector. The optical system which consists of lasers and optical filters sends the light signals to the detection area. The cytometer captures scattered light signals, fluorescence emissions from each cell and sends the signals to the electronic system. The

electronic system converts these sent light signals to electronic signals which are processed and measured by a computer.

From Figure 1.1 we can see, as the cells or particles flow through the detection region or cross the laser beams, they scatter and some fluoresce. The scattered laser beam sends the signals to the electronic system and particle volume and surface morphology are measured. With developments in techniques of micromachining, conventional cytometers which were bulky and complex are soon replaced by the miniature microfluidic flow cytometers.

1.1.2 Hydro-dynamic focusing

The main purpose of the fluidics system is to guide the sample flow or particles in the sample stream to the laser beams for detection. This is done by injecting the sample flow into the flow of sheath fluid within the flow cytometer. The flow chamber is designed in such a way that the sample or fluid that needs to be focused is in the center of the sheath flow. As the sheath fluid flows around the sample flow, it causes the particles to accelerate and restricts them in the middle of the sample core. This reduces the aggregation and allows the particles to flow in a single-file, where the laser is beamed and properties of particles or cells are studied. This phenomenon is known as hydrodynamic focusing. For the good reliable operation of the flow cytometer, hydrodynamic focusing is an important phenomenon that needs to be considered. Figure 1.1 shows the schematic representation of hydrodynamic focusing.

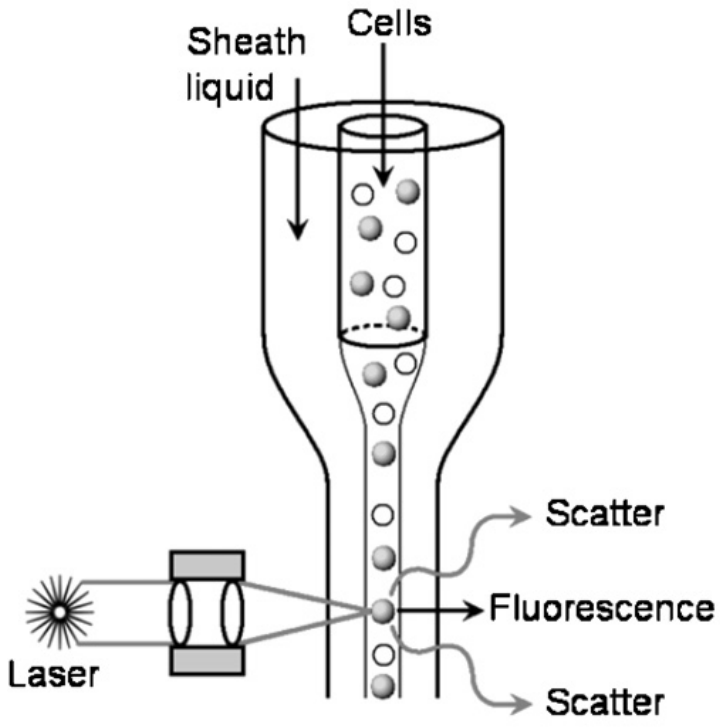

Figure 1.1 Schematic diagram of sample detection in a flow cytometer (Huh et al., 2005).

1.1.3 Particle focusing

Theoretically speaking, the particles need not be focused as it is possible to manufacture narrow channels and make the particles move in a single file and many researchers were successful in doing that. However these devices cannot be used if the application involves studying a large range of particle sizes and the narrow channels may cause clogging and surface fouling which is undesirable. Thus channels must be big enough to allow or accommodate large size particles to avoid clogging, which also means it can allow small particles, thus allowing studying the broad range of particles. As the sample flow is completely surrounded or sheathed by the sheath flow in the case of hydrodynamic focusing, the cells or particles do not come into contact with the walls of microfluidic device thus avoiding fouling and also damaging of the cells.

One dimensional focusing was achieved in past by introducing the sheath flow on either side of the sample flow focusing it laterally which was like a simple “cross” intersection (Figure 1.2). One of the major difficulties with the 1-D focusing is the efficiency of collection and uniformity of illumination. By focusing the sample flow in two and three dimensions, the particle can be made to flow or move one after the other in a single file, reducing the risk of damaging the walls of the channel and also cells.

1.1.4 Manufacturing

Fluidic components fabricated for flow cytometry are required to be on order of ten to hundreds of micrometers. Different techniques are used to fabricate the fluidic device like micromachining and lithography. Traditional ways of fabricating cytometer fluidic device

involved pulling a glass tube into very thin tubes and inserting a needle into the middle of the tube as an injector for the sample flow while the sheath flow flows around it.

1.1.5 Pumping/switching methods

For a stable and uniform flow fluid flow through the channel, the pumping techniques are to be considered. In old flow cytometers the flow is driven in the fluid chamber by creating pressure differences or by introducing the fluid at a constant flow rate using syringe pump. Modern cytometers use several pumping techniques. The pumping and switching processes can be divided into passive and active. Passive pumps are operated with no use of external power source. They are driven mostly by gravity, capillary force or evaporation (Huh et al., 2005). By maintaining height differences the liquids can be delivered through gravity (Simonnet et al., 2006). Effective pumping techniques were developed by Effenhauser et al. (2002) and a steady flow was maintained for days through the suction generated by the evaporation of the liquid. The surface tension of a small drop of liquid was also used to pump the liquid through a microchannel (Walker et al., 2002).

A large number of actively driven pumping systems are being used to pump the flow into the microfluidic device. One of the simplest techniques used in almost all the conventional cytometers is direct pneumatic pressure from external sources or by syringe pumps. Another technique is utilizing electric fields to move particles through the cytometer by electroosmosis or electrophoresis (Xuan et al., 2005). Lin et al.(2004) achieved a 3-D focusing of the sample flow by utilizing both hydrodynamic and dielectrophoretic forces (Figure 1.3). First two sheath flows are used to focus the sample flow in horizontal plane utilizing hydrodynamic force and then two embedded electrodes

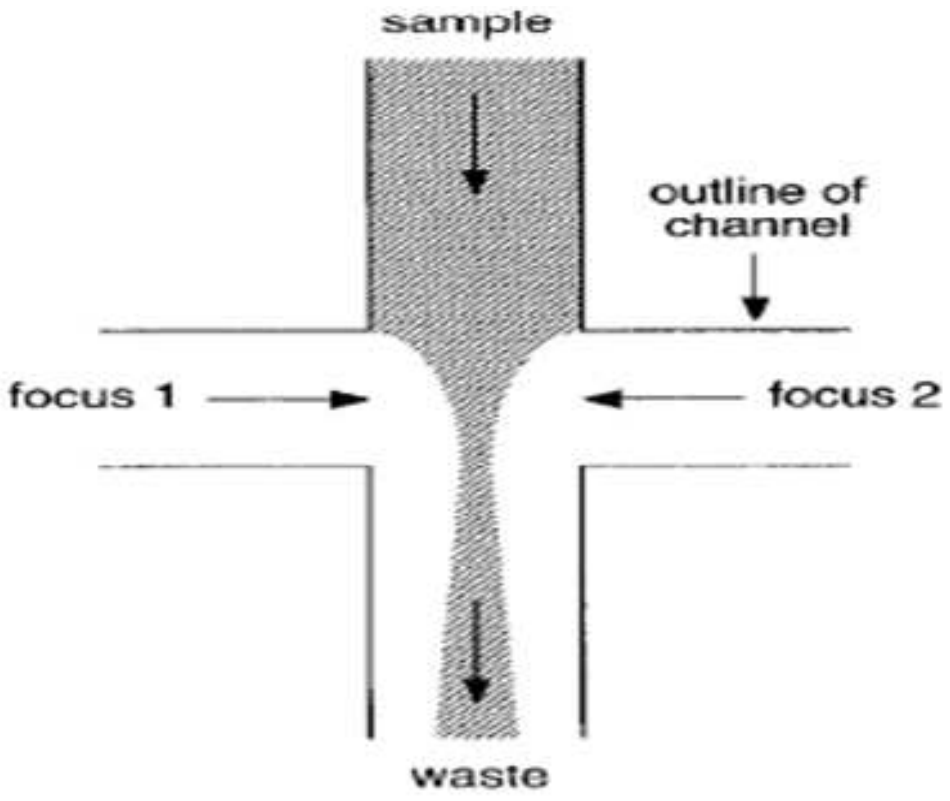

Figure 1.2 Schematic of 1-D focusing process (Jacobson and Ramsey., 1997).

makes the particles to focus vertically using dielectrophoretic forces.

1.2 Problem statement

The objective of this study is to simulate the flow inside a microflow cytometer and study the hydrodynamic focusing characteristics. A considerable amount of research in the field of microflow cytometry has been done concerned with the development of the different techniques for measuring and displaying photometric properties of various sample solutions. Effort was put to increase the accuracy of the device with interests in repeatability, sizing of the molecules. Little work has been done on studying the hydrodynamic behavior of the flow and to improve the design of microfluidic devices for flow cytometers. As the design of microfluidic device, hydrodynamic phenomenon, and fluid properties are related to performance of the cytometers, there is a need to study the effect of these conditions. With improvement in the techniques in the field of Computational Fluid Dynamics (CFD), microflows can be modeled accurately to study the flow behavior in the microflow cytometer to save time and money spent on manufacturing a prototype. In this work the hydrodynamic focusing characteristics of a microflow cytometer fabricated by Lee et al. (2001) were studied and the effect of flow conditions and physical properties of the fluids on the focusing width was investigated. CFD simulations were performed and results were compared with the experimental results available for this device. The particle motion in the flow cytometer and their focusing behavior were studied. The effect of the assumed geometry on the predicted focusing width with change in the flow rates was investigated.

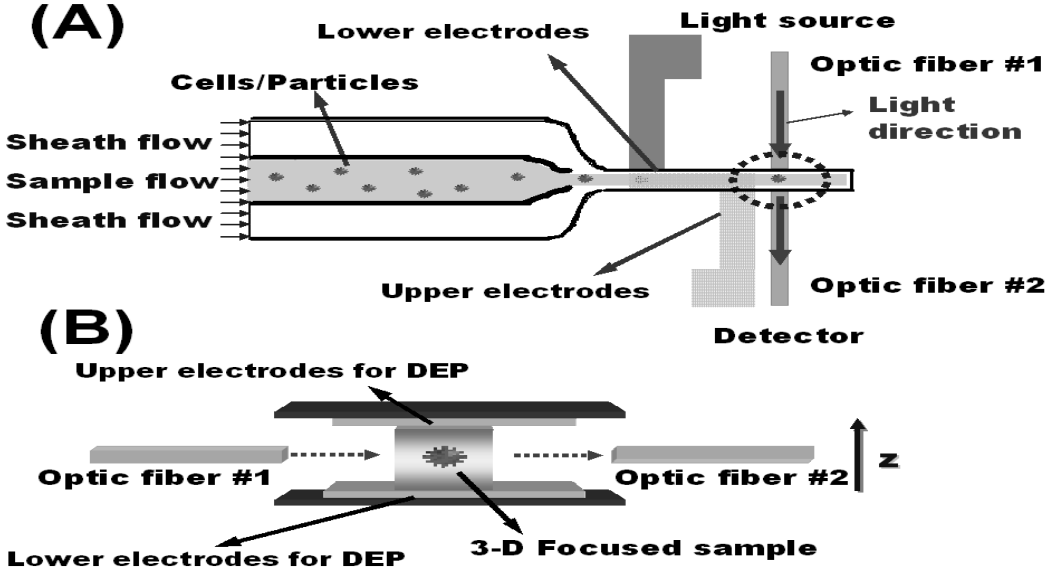

Figure 1.3 Schematic diagrams of the operating principles for 3-D focusing. (A) Top view and (B) side view. Cells/particles are focused at the center of the sample stream using dielectrophoretic (DEP) and hydrodynamic forces.(Lin et al., 2004).

1.3 Previous related studies

By focusing the sample flow in a two dimensions or in a 3-D, the cells or the particles can be forced to travel in a single file. With the development of many techniques in the field of micro-machining, optical and electrical systems, researchers come up with different models or devices utilizing these techniques. Some of the previous works done in this field are discussed here.

To enable three-dimensional focusing Mao et al.(2007) introduced a novel technique called “microfluidic drifting” with a simple single layer planar microfluidic device. Here 3-D hydrodynamic focusing was achieved in a two-step sequence. In the first step the sample flow is focused in the vertical direction by using a technique they called “microfluidic drifting”, in which the sample flow is laterally drifted by a transverse secondary flow induced by the centrifugal effect in the curve of microfluidic device. In the second step the vertically focused sample is compressed further horizontally by two horizontal sheath flows (Figure 1.4). Choi et al.(2008) demonstrated a microfluidic device for sheathless hydrophoretic focusing of microparticles with advantages of a sheathless method and passive pumping devices. They used slant obstacles which are placed in the device and acted as the source of hydrophoresis and the particles were separated by size (Figure 1.5). The channel area around the slant obstacles has less resistance to the flow than the flow direction and thus creating pressure gradient. Tsai et al.(2008) presented a three-dimensional hydrodynamic focusing technique with two pairs of sheath flows and a micro-weir structure. Here, first the sample flow is focused horizontally using a set of sheath flows and then vertically by using another set of sheath flow and a micro-weir structure. Performed numerical simulations revealed that the 3-D

focusing approach not only made cell/particles focused horizontally but also separated them in the vertical plane so that they flow one by one through the detection regions (Figure 1.6). Lee et al.(2010) reported a contraction-expansion array (CEA) microchannel that produces the 3-D hydrodynamic focusing. Numerical simulations were carried out using a commercial CFD solver and the results were compared with the experimental. Sheath and sample fluids are fed into the device where they flow through the contraction and expansion region and finally at the end the sample fluid is wrapped by the sheath flow (Figure 1.7). Numerical simulations were carried for different flow rates, flow ratios and their effects on focusing width were studied. Chang et al.(2007) designed and fabricated a three-dimensional hydrodynamic focusing microfluidic device (Figure 1.8). Here, first the sample fluid was focused vertically and then horizontally making it more suitable for cell counting when compared to two dimensional hydrodynamic focusing. Computational Fluid Dynamics (CFD) simulations were carried out for different aspect ratio (height/width) of vertical focusing channel and its effects are studied and also the influence of the flow rates on the formation of core-sheath structure are explained. Computational fluid dynamics (CFD) simulations were done based on finite volume methods using commercially available software. The performance of the device was confirmed by conducting simulations for various Reynolds numbers of 0.5, 1.0, 5.0 and 10.0. Yang et al. (2007) carried out CFD simulations to study the phenomena of hydrodynamic focusing in microflow cytometry. Ten numerical experiments were conducted and the results obtained were in good agreement with the experimental results of Lee et al. (2001).

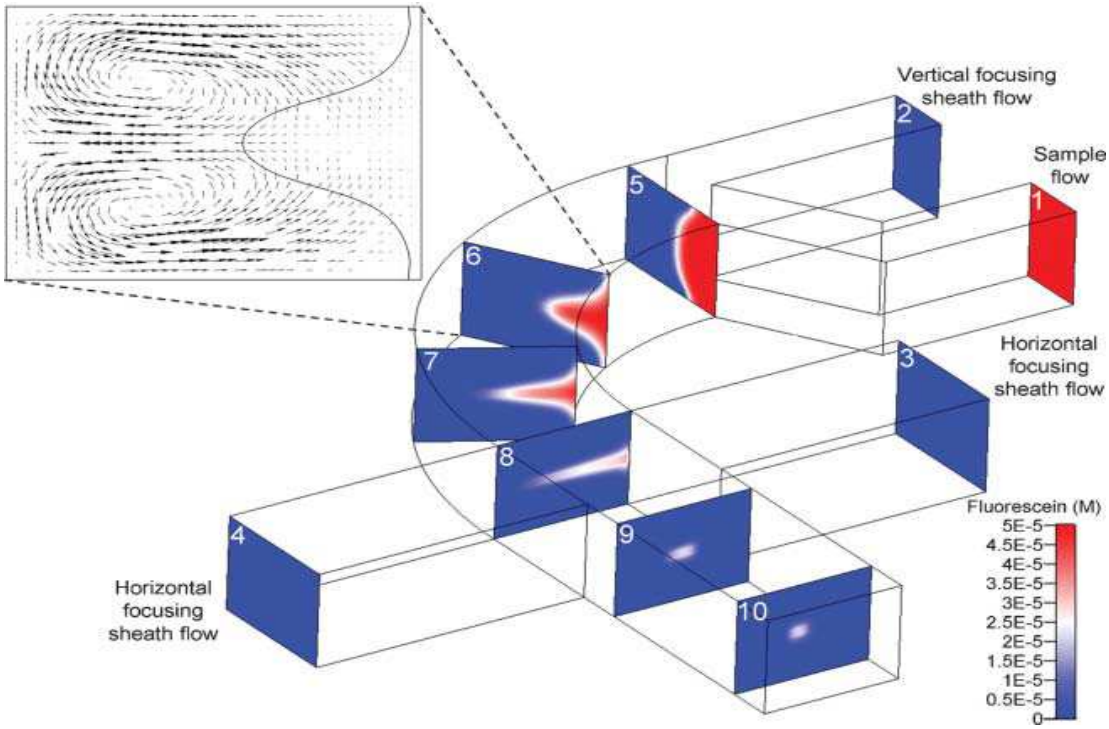

Figure 1.4 Schematic of the 3D hydrodynamic focusing process by employing the ‘‘microfluidic drifting’’ technique. Inset: the simulation of the secondary flow velocity field shows the formation of Dean vortices in the 90-degreee curve.(Mao et al., 2007).

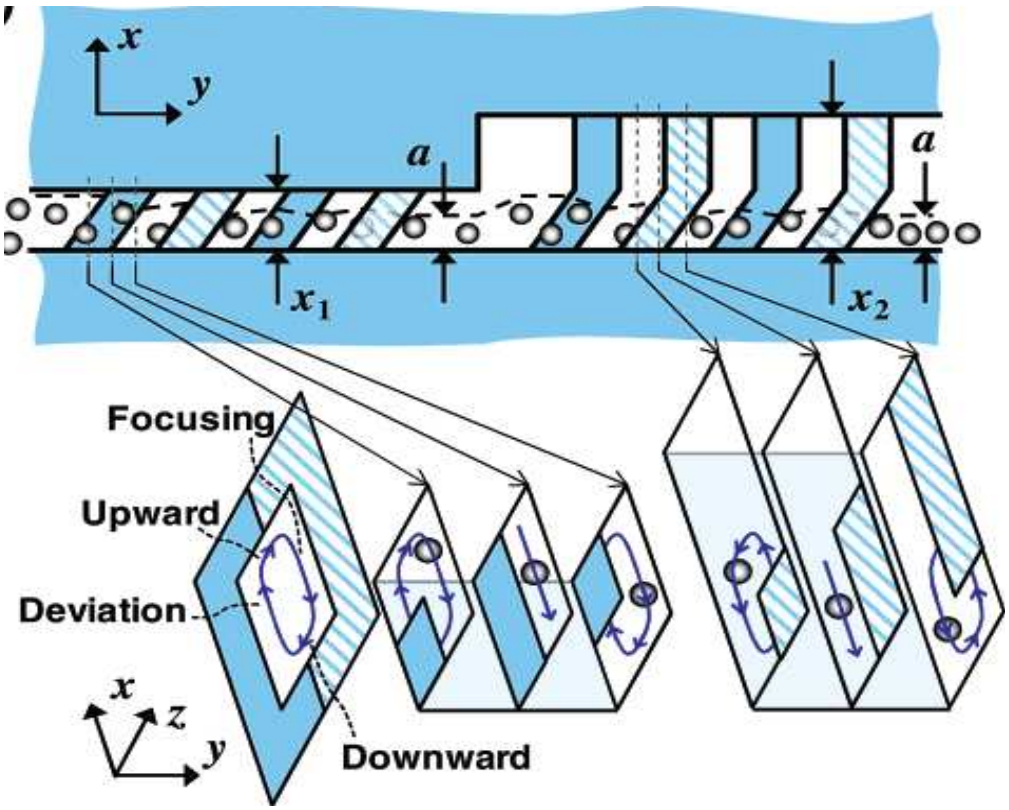

Figure 1.5 Schematic diagrams showing the focusing procedures of particles. Colored and lined areas denote lower and upper PDMS layers, respectively (Choi and Park., 2007).

The experiments were conducted by varying the velocity ratios of the both the sheath and sample flow and the effect of this ratio on the focusing width and length were studied. The increase in the sheath to shell velocity ratio resulted in a decrease in the width and the length of the focusing area. The pressure drop of sample stream across the inlet and outlet of the micro flow device was observed and results showed that there is a gradual increase in the pressure drop as the ratio of sheath to sample flow velocity is increased. Lee et al. (2001) investigated the hydrodynamic focusing phenomenon by using potential flow theory; the flow inside the microfluidic device is simulated numerically. The effect of microfluidic device geometry and velocities of the sheath and sample flows on the focusing width were studied. From the experimental data, they concluded that the size or width of the focused stream is considerably reduced by changing the velocity ratios of sheath and core steams.

Hydrodynamic focusing eliminates the use of small nozzles which may cause clogging in the case of polymer solutions or large particles. Srivastava et al. (2008) electrospun core-sheath structured nanofibers using hydrodynamic fluid focusing by molding a microfluidic 2D-flow focusing devices in PDMS elastomer. Core fluid entering the central microchannel at the A–B junction, is initially focused in the vertical direction at the A–C junction, and subsequently focused laterally into a single stream at the A–D junction prior to exiting the device (Figure 1.9). Thangawng et al.(2009) produced micro and nanofibers with controlled sizes and shapes using hydrodynamic focusing in a microfluidic sheathing device avoiding use of nozzle as in electrospinning method (Figure 1.10). Straight, diagonal and chevron-shaped grooves integrated into the walls of channels directed the sheath fluid around the core stream in a well-defined path.

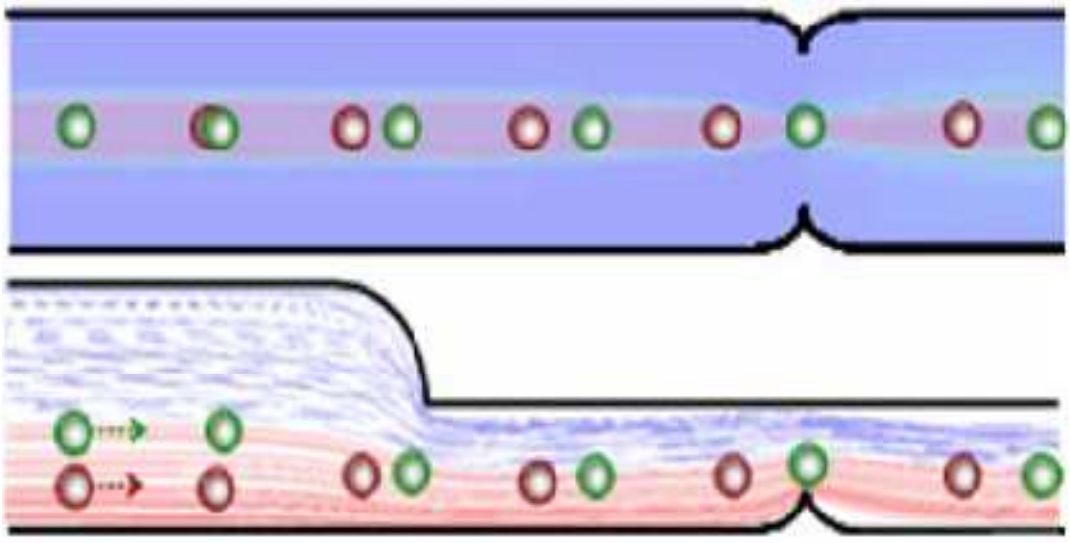

Figure 1.6 Numerical trace results for micro-particle distributions in(a) X-Y and (b) X-Z planes (Tsai e t al., 2008).

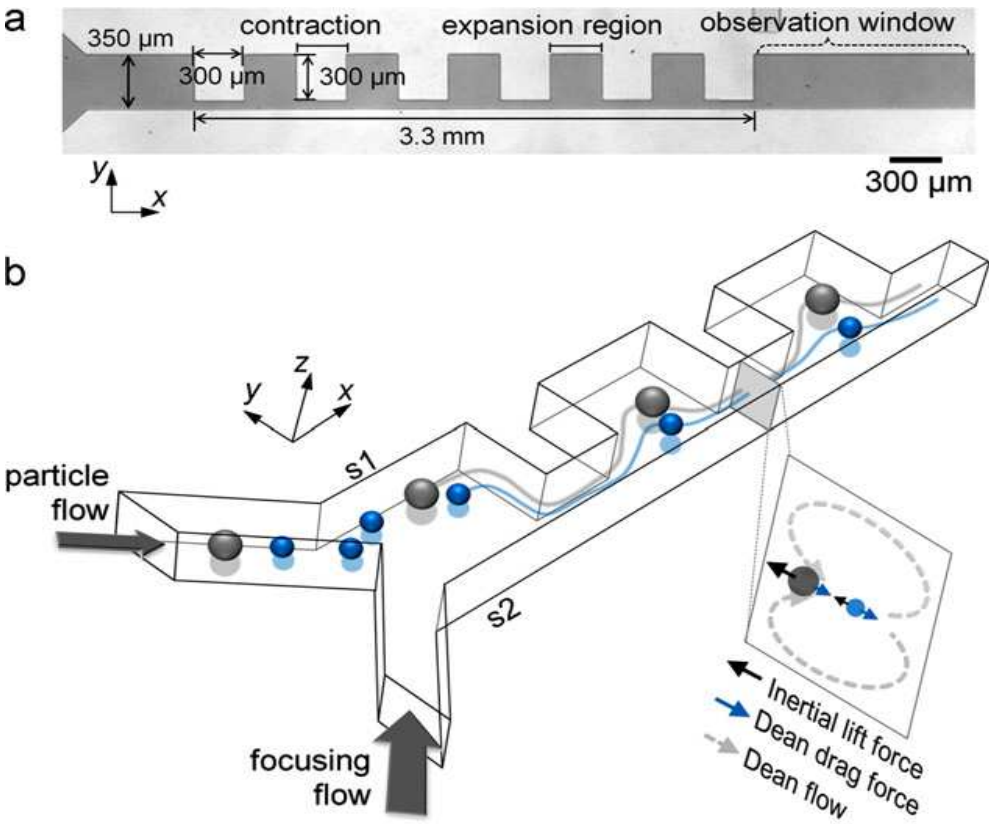

Figure 1.7 Contraction–expansion array (CEA) microchannel (Lee et al., 2010).

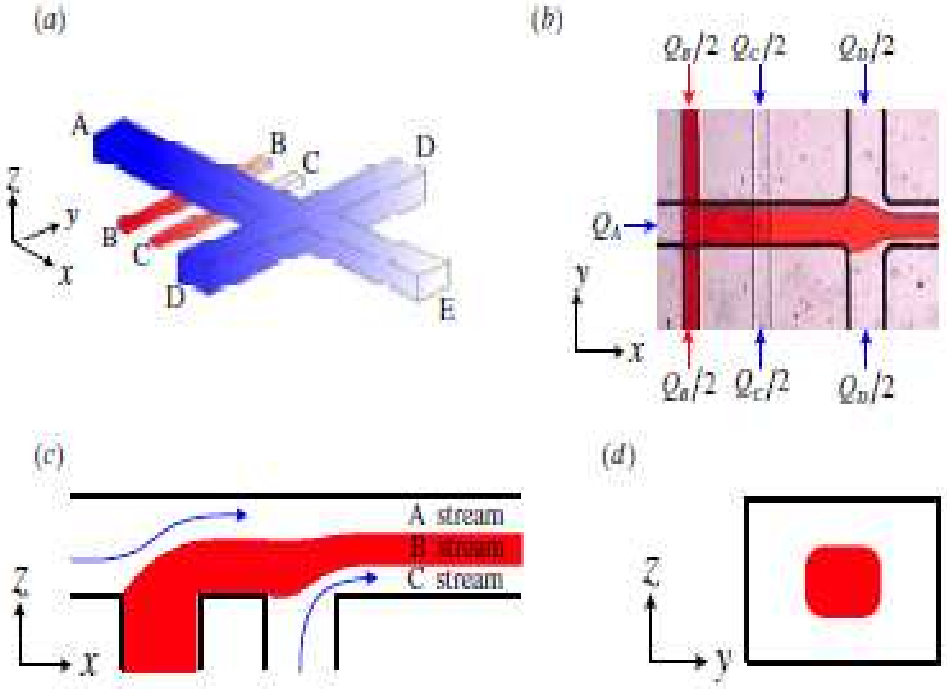

Figure 1.8: Schematic illustration of the three dimensional hydrodynamic focusing device. (a) 3D view, (b) top view, (c) side view and (d) cross-section perspective (Chang et al., 2007).

1.4 Specific objective

The objectives of the present study are:

- To perform numerical simulations of the flow in a microflow cytometer to study its hydrodynamic focusing behavior. The Microfluidic device considered in this work was fabricated and tested by Lee et al. (2001)
- To investigate the effects of the velocity ratios of the sheath and sample streams on focusing width.
- To investigate the hydrodynamic focusing phenomenon by injecting particles into the microfluidic device and to study their motion.
- To determine the focusing characteristics of non-Newtonian fluids in comparison with Newtonian fluids.

1.5 Organization of thesis

The present study is divided into four chapters. Introduction to cytometry and its working principles, manufacturing techniques; pumping devices were explained in chapter 1.

Chapter 2 explains the computational methods used to perform the numerical simulations. The models used, geometry description and meshing details are explained. The Chapter concludes with explaining numerical results obtained from the simulations performed and its validation with the experimental results from literature is also shown.

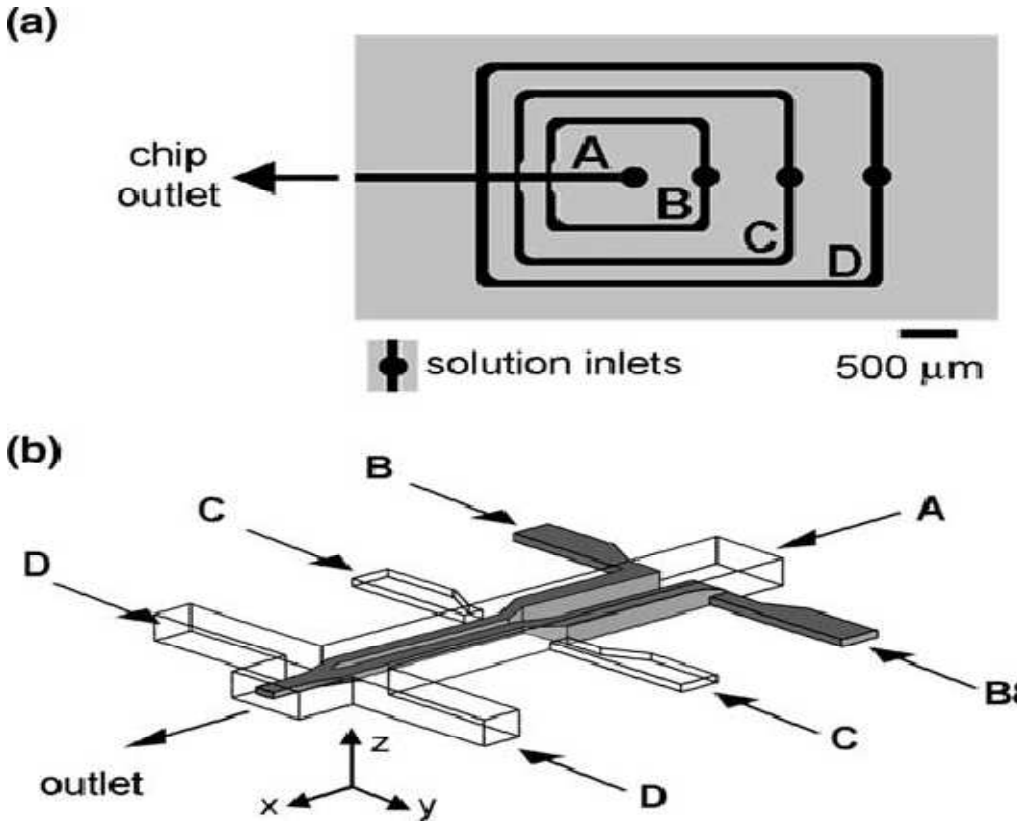

Figure 1.9 (a) Schematic representation of the microchannel layout in the PDMS 2D flow-focusing device. (b) Illustration of the 2D flow focusing process in the microfluidic device (Srivastava et al., 2008).

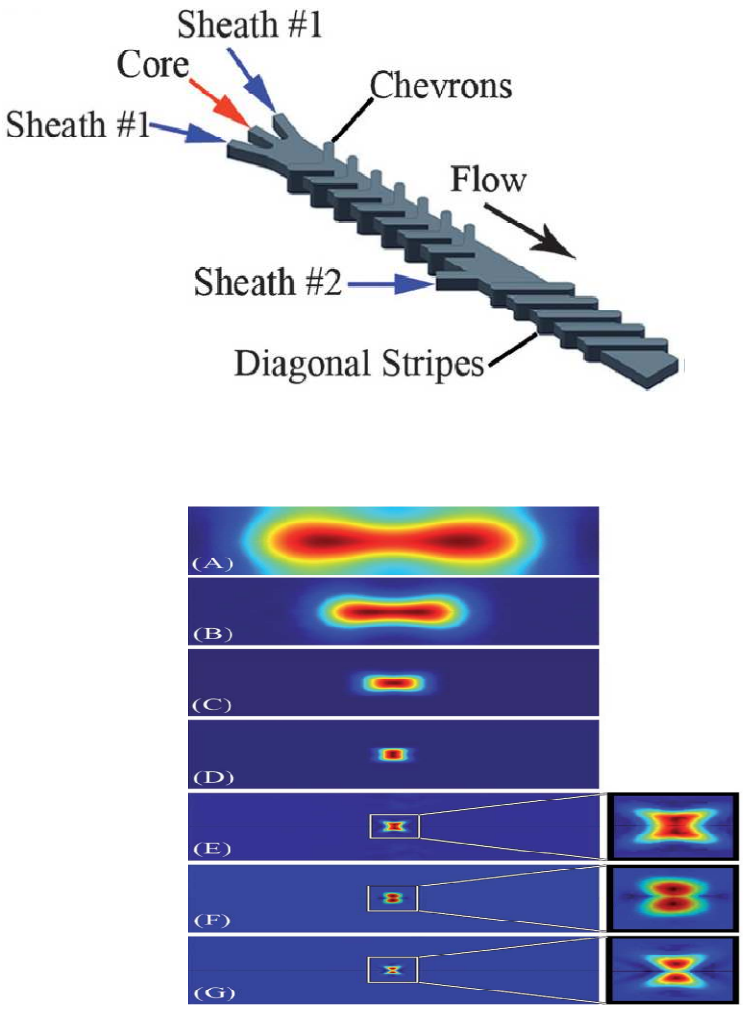

Figure 1.10 (Top) 7 chevron/5-diagonal groove combination design for shaping and size reduction (Bottom)COMSOL Multiphysics simulation of the shape of the core stream for a 7 chevron device at a sheath-to-core flow-rate ratio of (A) 1:1, (B) 5:1, (C) 25:1, (D) 100:1, (E) 500:1, (F) 1000:1, and (G) 2500:1(Thangawng et al., 2009).

Chapter 3 provides the results obtained by performing numerical simulation. Particle tracking in the cytometer and the effect of sample fluid physical properties on the focusing behavior are discussed. The non-Newtonian model of blood is considered and change in the focusing width compared to Newtonian sample flow is presented

Chapter 4 ends with the conclusion of this work and the recommendations and scope for the future work that can be done in this field.

Chapter II

COMPUTATIONAL METHODS

2.1 Introduction

In this study, numerical simulations were performed to explore the focusing behavior in a micro-flow cytometer. Computational Fluid Dynamics (CFD) code FLUENT 12.0 is used to study the flow behavior of the sample and the sheath flows. Simulations were validated against the experimental results of Lee et al.(2001). The flow cytometer used by Lee et al. (2001) was fabricated on PMMA substrate using a hot embossing method.

2.2. Geometry

Figure 2.1 shows the schematic diagram of the two dimensional microflow cytometer. The overall length of the nozzle or computational domain is 20 mm with inlet width of 3.6 mm and 2.4 mm for the outlet section. The microfluidic device consists of three channels where the sample flow is introduced from the center channel and sheath flows from upper and lower channels, where the sample flow from center channel is focused hydrodynamically after it exits the center channel. The length of the inner nozzle is 11 mm in this study, while the thickness of the wall is 0.21 mm and the width at the exit of the inner nozzle is 0.6 mm. Lee et al. (2001) performed numerical experiments changing the location of the inner nozzle and found that the focused stream is a strong

function of the length of the inner nozzle. The geometric parameters of the microflow cytometer are given in the Table 2.1.

The geometry of the nozzle is a critical parameter and the profile of the convergent part plays a crucial role in determining the focused stream. Figure 2.2 shows the close-up schematic view of the convergent part and the profile of the inner and outer nozzle convergent part is given by the equations 2.1 and 2.2 (Lee et al.2001). Interestingly the nozzle profile was used before by Morel et al.(1975) where the wall shape was formed of two smoothly joined cubics which was a suitable choice for a wall contour for axisymmetric wind tunnel contractions.

(1) $l < Lm$

$$r = (r_1 - r_2)\left[1 - \frac{(l/Lc)^3}{\left(\frac{Lm}{Lc}\right)^2}\right] + r_2 \qquad (2.1)$$

(2) $l > Lm$

$$r = (r_1 - r_2)\left[\frac{(1-l/Lc)^3}{\left(1-\frac{Lm}{Lc}\right)^2}\right] + r_2 \quad , L_m = L_C/2 \qquad (2.2)$$

r_1	r_2	$D_1=D_2=D_3$	D	L_1	L_2
0.6	0.3	1.2	2.4	10	8

Units in mm

Table 2.1 Geometric parameters for the flow cytometer.

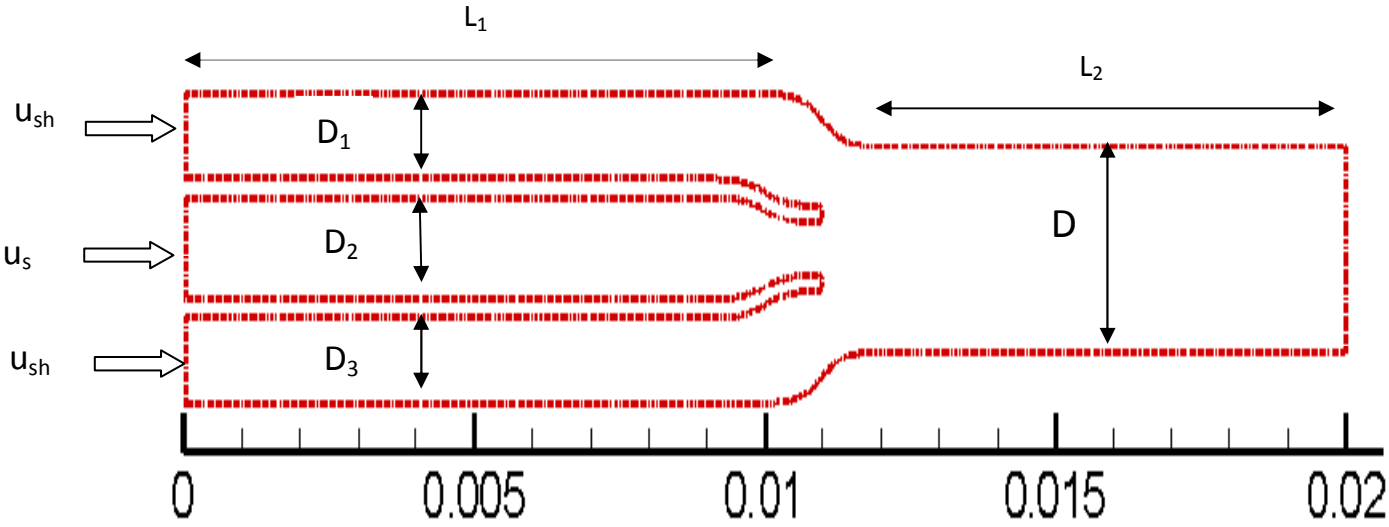

(a)

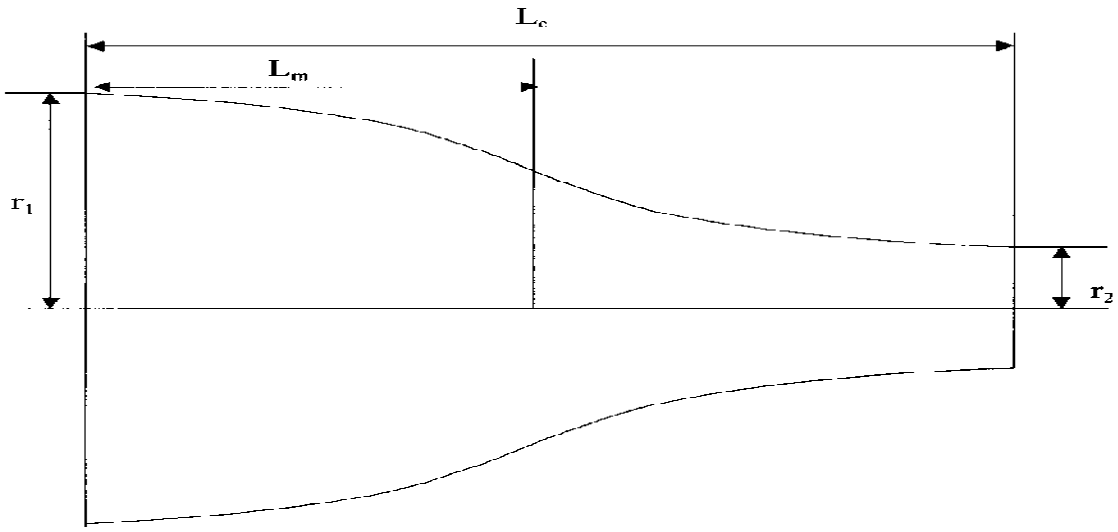

(b)

Figure 2.1 (a) Schematic representation of the micro flow cytometer (b) Close-up schematic of the convergent nozzle (Lee et al., 2001).

2.3 Numerical approach

A series of simulations were performed using commercially available CFD code ANSYS FLUENT 12.0 and the numerical results were validated using the experimental results obtained by Lee et al. (2001). In this simulation, the flow field was modeled using 2-D Navier-Stokes equation. The following assumptions were made to simplify the mathematical equation without affecting the physics associated with it:

Assumptions:

1. Two-dimensional flow is considered.
2. The flow is Newtonian, steady, laminar, and incompressible.
3. No-slip condition on solid walls
4. Isothermal flow.
5. Neglecting the forces from gravity.

2.4 Multiphase models

ANSYS FLUENT numerically solves different multiphase flows by two approaches, one Euler-Lagrange approach and other Euler-Euler approach. In the Euler-Lagrange approach primary phase or fluid phase is solved by Navier-Stokes equation while the dispersed phase is solved by tracking particles through the flow. This model cannot be used when the volume fraction of the dispersed phase is not negligible; as the main assumption in this approach is that the dispersed phase occupies a small volume fraction. In the Euler-Euler approach, the fluids are treated as interpenetrating continua where the phases are dispersed randomly in space and time. The sum of the volume fractions is taken as obviously one.

The three Different Euler-Euler multiphase models available in ANSYS FLUENT are:-

1. Volume of Fluid (VOF) model
2. The Mixture model
3. Eulerian Model

Volume of Fluid (VOF) model in ANSYS FLUENT is an Eulerian-based method useful to solve the flow of two immiscible fluids where the interface between the fluids needs to be studied. The fraction of the first fluid is 1 if the cell is filled with fluid and 0 if the cell is empty. The function values between 0 and 1 contain free surface between the fluids. Stratified flows, free surface flows and predicting jet breakup can be solved using VOF model.

Since there are only two kinds of fluids present, the sum of volume fractions of the fluids is equal to 1.

$$\alpha_p + \alpha_q = 1 \tag{2.3}$$

There are some limitations when using VOF model in ANSYS Fluent. The VOF model is available only with the pressure based model and density based solver cannot be used. This model also does not allow void regions where cell is not filled with any fluid.

The continuity equation for the volume fraction of the phase is given (fluent, Inc.) by:

$$\frac{1}{\rho_q}\left[\frac{\partial}{\partial t}\left(\alpha_q \rho_q\right) + \nabla.\left(\alpha_q \rho_q \overline{v_q}\right) = S_{\alpha_q} + \sum_{p=1}^{n} \dot{m_{pq}} - \dot{m_{qp}}\right] \tag{2.4}$$

where α_q is the q[th] fluid volume fraction, ρ_q is the density and $\overline{v_q}$ is the velocity vector of the q[th] fluid, $\dot{m_{pq}}$ is the mass transfer from phase p to phase q and m_{qp} is the mass transfer from the phase q to the phase p. By default the right side term from above equation is zero. A user defined function (UDF) or constant mass source for each phase can be specified if needed. Thus the equation becomes:

$$\frac{\partial}{\partial t}\left(\alpha_q \rho_q\right) + \nabla.\left(\alpha_q \rho_q \overline{v_q}\right) = 0 \tag{2.5}$$

The momentum equation is given by

$$\frac{\partial}{\partial t}(\rho\,\overline{v}) + \nabla.(\rho\,\overline{v}\,\vec{v}) = -\nabla \mathrm{p} + \nabla.\left[\mu\left(\nabla\overline{v} + \nabla\overline{v}^{T}\right)\right] + \rho\vec{g} + \vec{F} \tag{2.6}$$

2.5 Grid

This 2-D geometry was constructed by using pre-processor ICEM CFD with hexahedral grids. Grid independence check was performed using three values of mesh size to ensure the solution does not depend on the mesh. Numerical computations were performed using 483k, 810k, 892k cells to ensure the solution is grid independent. The solution obtained was grid independent and a grid size of 892k cells was used in the present study. Finer grids were placed at the convergent part of the nozzle to resolve the sudden variations in the flow properties which also affects the focusing phenomena. The dimensions for the convergent part of the nozzle were calculated using the equation given by equations 2.1 and 2.2 and to get the smooth profile of the convergent part, points were obtained for an increment of 0.05 mm of the distance from the start of the convergent part of the nozzle. The schematic view of the mesh setup is shown in the Figure 2.2 for the 2-dimensional microfluidic device.

2.6 Boundary conditions

The boundary conditions are set for the two inlets, the outlet and wall. The axial velocity of incoming sample and sheath flows are assumed to have uniform profiles. Stationary and no-slip condition with zero normal gradient of pressure is set along the walls. Velocity inlet boundary conditions were assigned to both the sample and sheath flows entering into the nozzle. Pressure outlet condition was assigned at the outlet.

2.7 Numerical simulation procedures

The flow in the microfluidic device is considered as laminar and two fluids flow next to each other in this device. No turbulence occurs and molecular mixing between the two fluids is considered negligibly small. Because there are two fluids involved in the simulation, the flow system in ANSYS FLUENT is considered as a multiphase flow system and Volume of Fluid model (VOF) (Hirt and Nichols,1981) is used to simulate the flow. The governing equations for the two fluids are given by equations 2.5 and 2.6. The interfacial tension force is neglected as the flow is driven by the external pressure.

2.8 Problem setup

The mesh is read into Fluent and a grid check is performed to check for skewness and negative volumes. After the mesh check performed is success, the material properties are described. The sheath and the sample flow material are chosen as water liquid solution. The density and viscosity of the sample and sheath water is 998 kg/m^3 and 0.001 $N\text{-}s/m^2$.

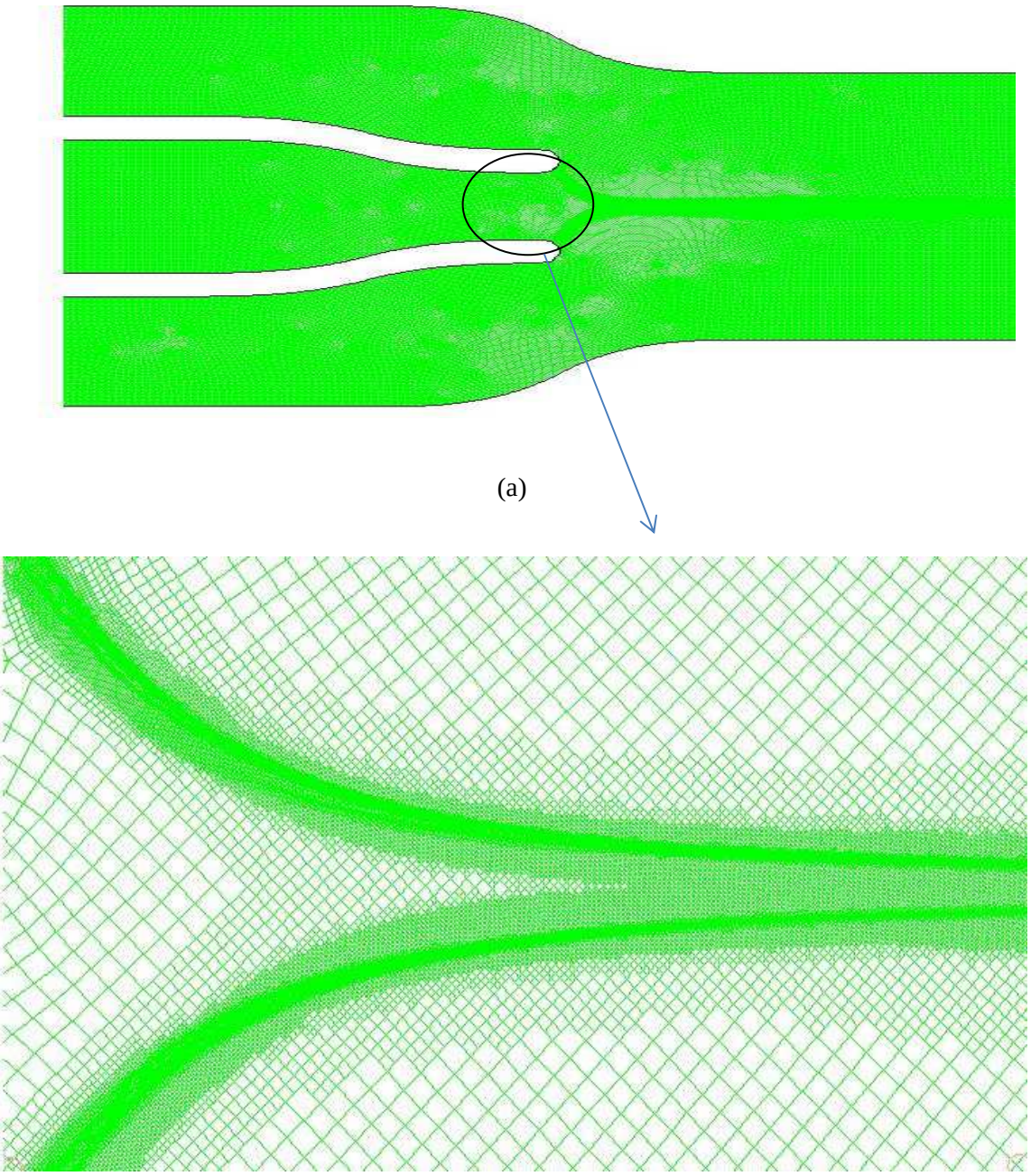

(a)

(b)

Figure 2.2 (a) Generated mesh of the flow cytometer. (b) Enlarged view of the mesh setup for the outlet section of the microflow cytometer with adapted grids on the basis of volume fraction (rectangular dimension of 0.57 mm *0.34 mm).

VOF model is chosen from the available multiphase models with implicit scheme of two phases. The sheath water is chosen as a secondary phase and the sample as the primary phase. The boundary conditions are set as described earlier and volume fraction of the sample and the sheath are defined. The volume fraction of the sheath flow is set to 1 for the upper and lower channel flows and 0 for the center channel flow (i.e. the sample flow). The equations were solved by choosing SIMPLEC (Semi-Implicit Method for Pressure-Linked Equations Consistent) scheme for pressure-velocity coupling. Second order upwind spatial discretization for both momentum and volume fraction is chosen as the solution method. For every steady state calculation the residual errors of variables are made to converge to 10^{-9}. To investigate the hydrodynamic focusing, the velocity of the sample fluid (u_s) in the center channel of the cytometer is maintained at 0.002 mm/s whereas the sheath water velocity (u_{sh}) is varied with values of 0.1 mm/s, 0.3 mm/s, 1.0 mm/s and 1.4 mm/s. The mesh was refined at the corners and at the interface of sample and sheath flows to measure the focusing width using the adaptation feature of FLUENT. From the obtained results, the grid independence is achieved and to measure the focusing width which is decreasing with increase in velocity ratios, the grid needed to be refined for highest velocity ratio of 70 to resolve the focusing width which is in order of less than 10 microns.

2.9 Validation of numerical results

After the solution is converged, the velocity and pressure fields are plotted. Figure 2.3 shows the velocity vector plot in the micro-flow cytometer for velocity ratios of sheath to sample flow (u_{sh}/u_s) of 50 and enlarged view at the exit of the inner nozzle is also shown. At the inlet both the sample and sheath flow velocity is uniform with Reynolds number of

1.2 calculated using the sheath flow velocity at the inlet. As the sample and sheath fluids flow downstream, due to no-slip condition the velocity at the wall is zero. Thus the fluid at the center of the channel has the highest velocity changing the flow into a parabolic profile. Figure 2.4 shows the velocity profile plotted against the transverse direction at the location of 11.2 mm along the x-direction for velocity ratio (u_{sh}/u_s =50). At this location the parabolic profile of both sheath and sample can be seen with peak velocity of the sheath flow at 1.5 mm/s surrounding the sample fluid at the exit of the inner nozzle. The graph shows a large velocity gradient at the interface between the sample and sheath flow fluids. This large velocity gradient causes the sample flow to accelerate, stretch and thereby reduce its width thus exhibiting the hydrodynamic focusing phenomena. This phenomenon can be seen in Figure 2.5, where the contours of volume fraction of the sample fluid are displayed for the velocity ratio (U_{sh}/U_s) of 5. Stretching, reduction in width and focusing phenomenon can be seen in Figure 2.6 for different velocity ratios (u_{sh}/u_s=5, 15, 50, 70). We can see the volume occupied by the sample fluid after exiting the inner nozzle is reduced as velocity ratio is increased. Figure 2.7 shows that the pressure decreases with the axial distance from inlet to the outlet of microflow cytometer. As the two fluids merge at the exit of the inner nozzle, the high velocity sheath fluid creates pressure gradient and thus compresses the sample fluid. In turn the low pressure can make cells or the other particles transported with the sample fluid stay in the core region and move along the centerline.

The focusing width is measured at the outlet by plotting the volume fraction of the sample fluid and considering iso-contour of α_s= 0.5 along the transverse direction. Figure 2.8 shows the data of the volume of fluid occupied by sample along the outlet. This is

repeated for velocity ratios of 5, 15, 15, 70 and the focused width is calculated. The obtained values of focused width are plotted against the velocity ratios. Figure 2.9 shows the variation of the focused width with change in the sheath flow rate for the velocity ratios of sheath to sample of 5, 15, 50, and 70 compared with the experimental results of Lee et al. (2001). As the velocity ratio is increased the focusing width is reduced which is commonly observed in the flow cytometer. At the velocity ratio of 5 the predicted focused width is 176 µm and as the sheath flow rate is increased, the increase in the velocity gradient compresses the sample fluid exiting the inner nozzle. From the obtained numerical results it can be seen that the focusing width can be reduced to around 10 µm at a velocity ratio of 70. Generally the size of blood cells range from 5 µm to 15 µm, so to sort and count the cells it is required that the width of focused sample fluid is maintained around 15 µm. From the results obtained, the focusing width of 15µ m can be achieved by maintaining the velocity ratio of 50. The predicted results match well with the experimental results of Lee et al. (2001) with errors of 1.6% and 4.8%for velocity ratios of 5 and 15 respectively. Above simulations were performed on a 2-D geometry, a symmetry plane could have been used to save the computational time but the present mesh was favored because it could be used to solve the focusing of complex particle/molecule that would not result in a symmetric flow.

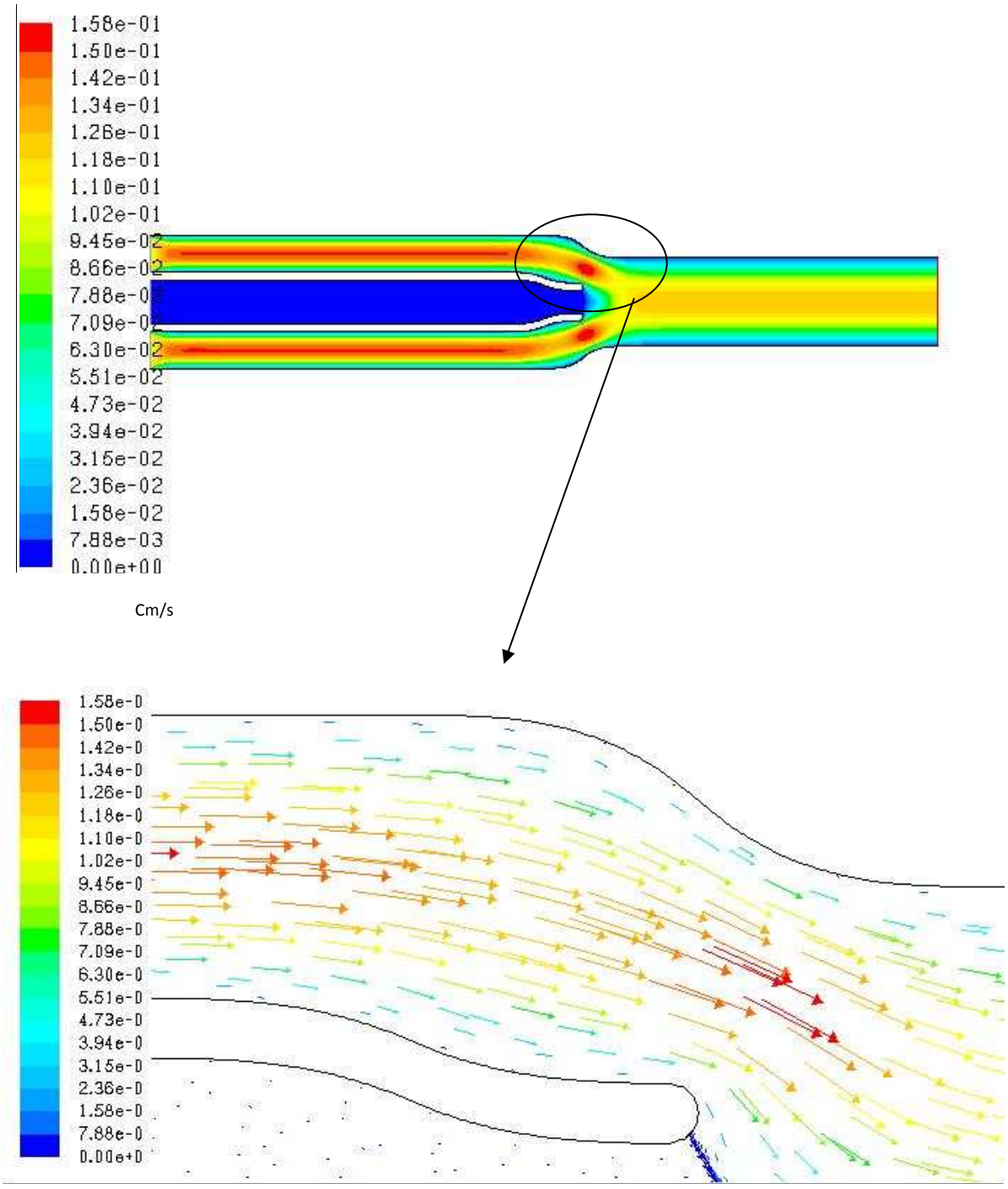

Figure 2.3 (a) Velocity vector plot of the micro-flow cytometer at velocity ratio (u_{sh}/u_s =5). (b) Enlarged view at the exit of the inner nozzle (with 150 skipped vectors).

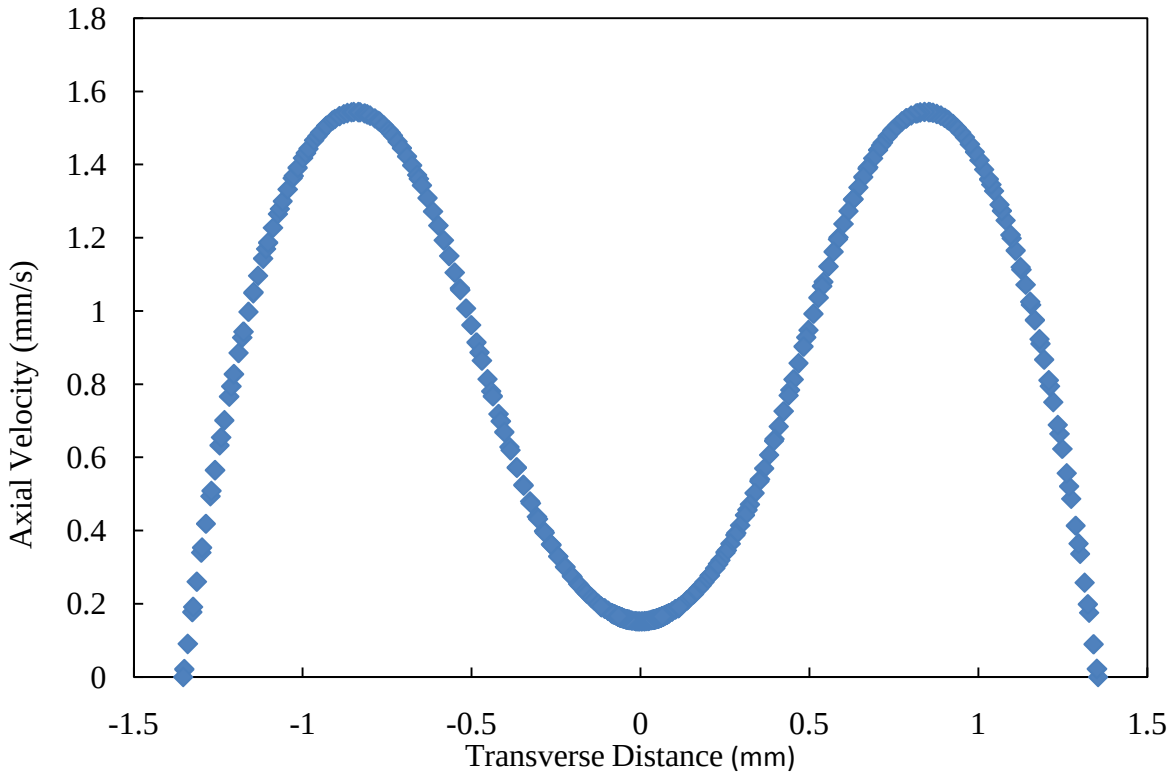

Figure 2.4 Plot showing the axial velocity distribution at the transverse location of 11.2 mm for the velocity ratio (u_{sh}/u_s=5).

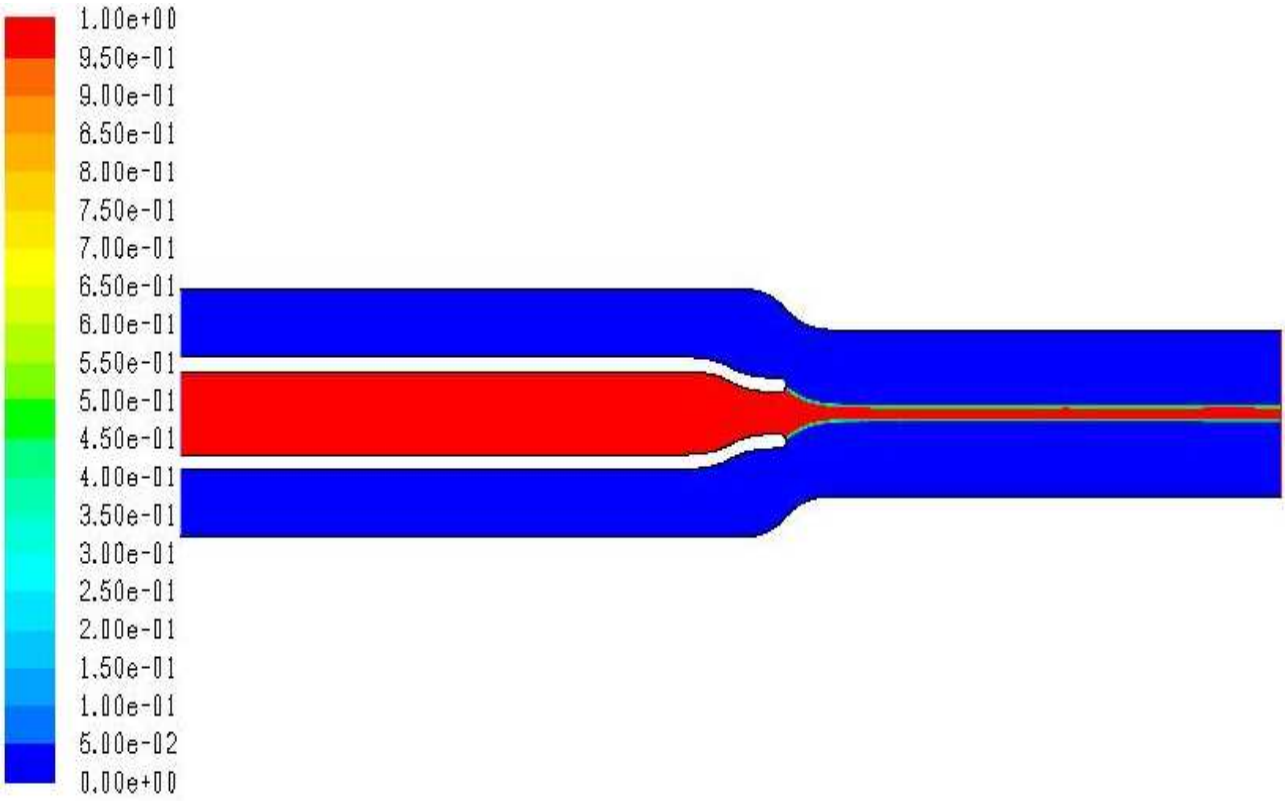

Figure 2.5 Contours of the volume fraction of the sample fluid (u_{sh}/u_s =5).

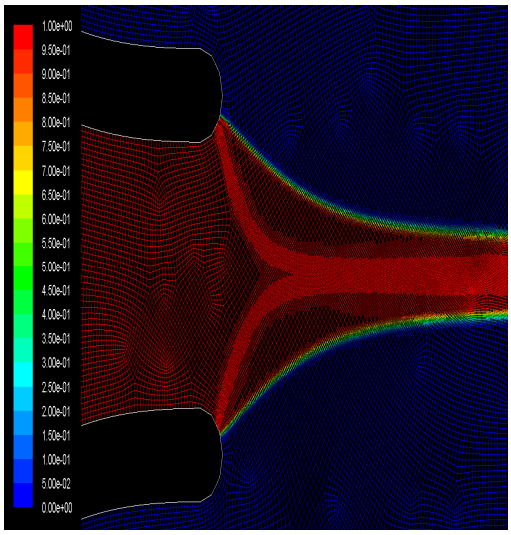

Velocity ratio (u_{sh}/u_s=5)

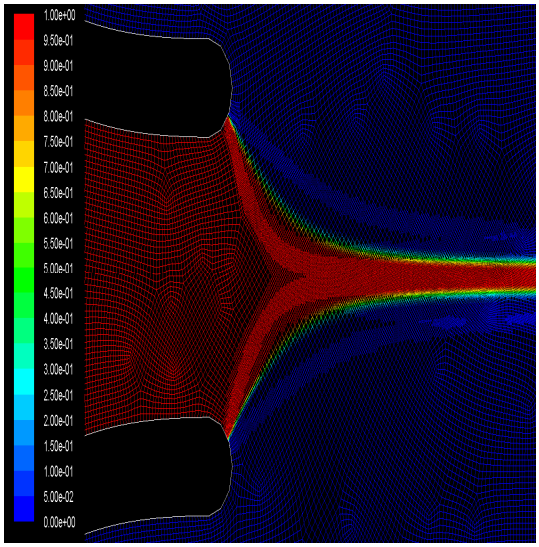

Velocity ratio (u_{sh}/u_s=15)

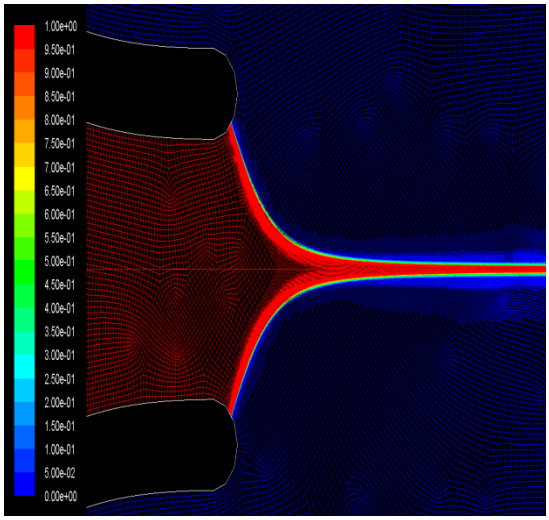

Velocity ratio (u_{sh}/u_s=50)

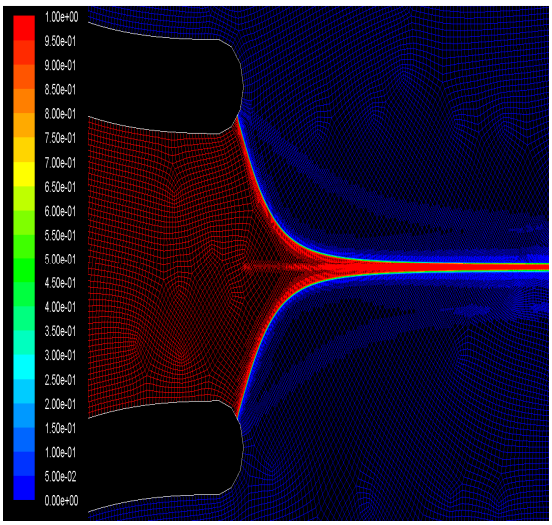

Velocity ratio (u_{sh}/u_s=70)

Figure 2.6 Enlarged view of the volume fraction contours of the sample fluid of flow cytometer at the exit of the inner nozzle for different velocity ratios.

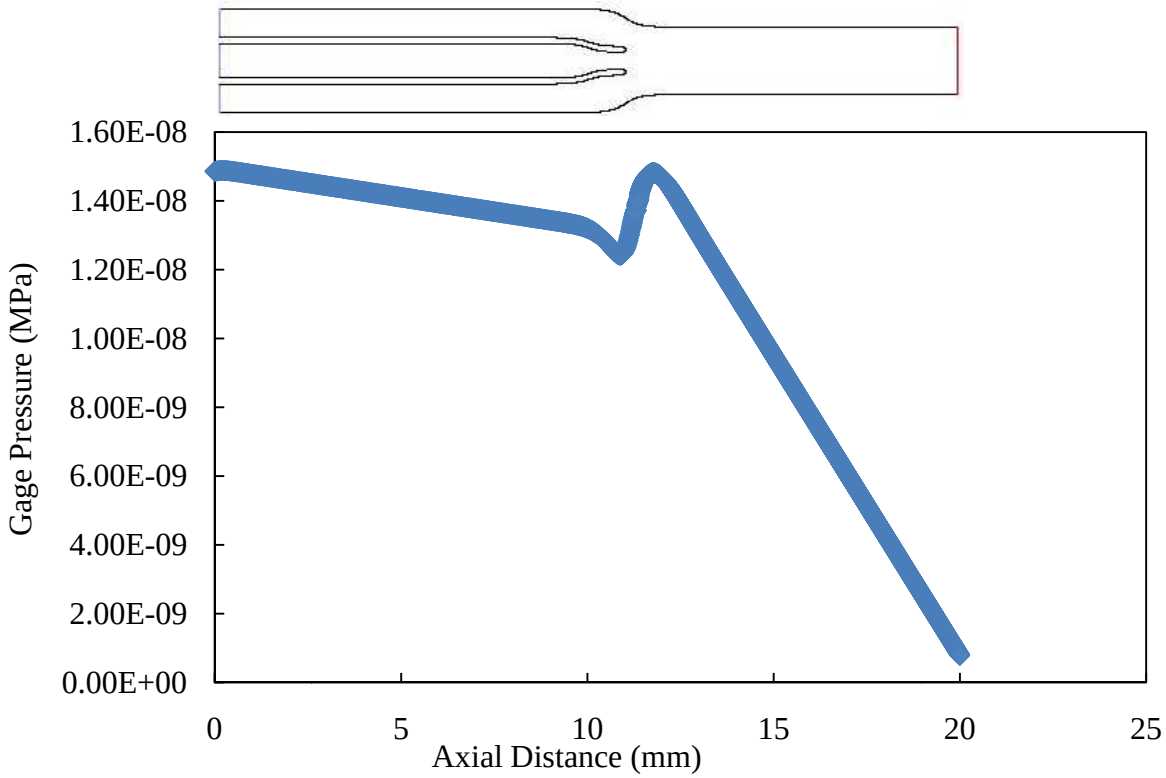

Figure 2.7 Pressure profile along axis (Centerline) of micro flow device (u_{sh}/u_s= 15).

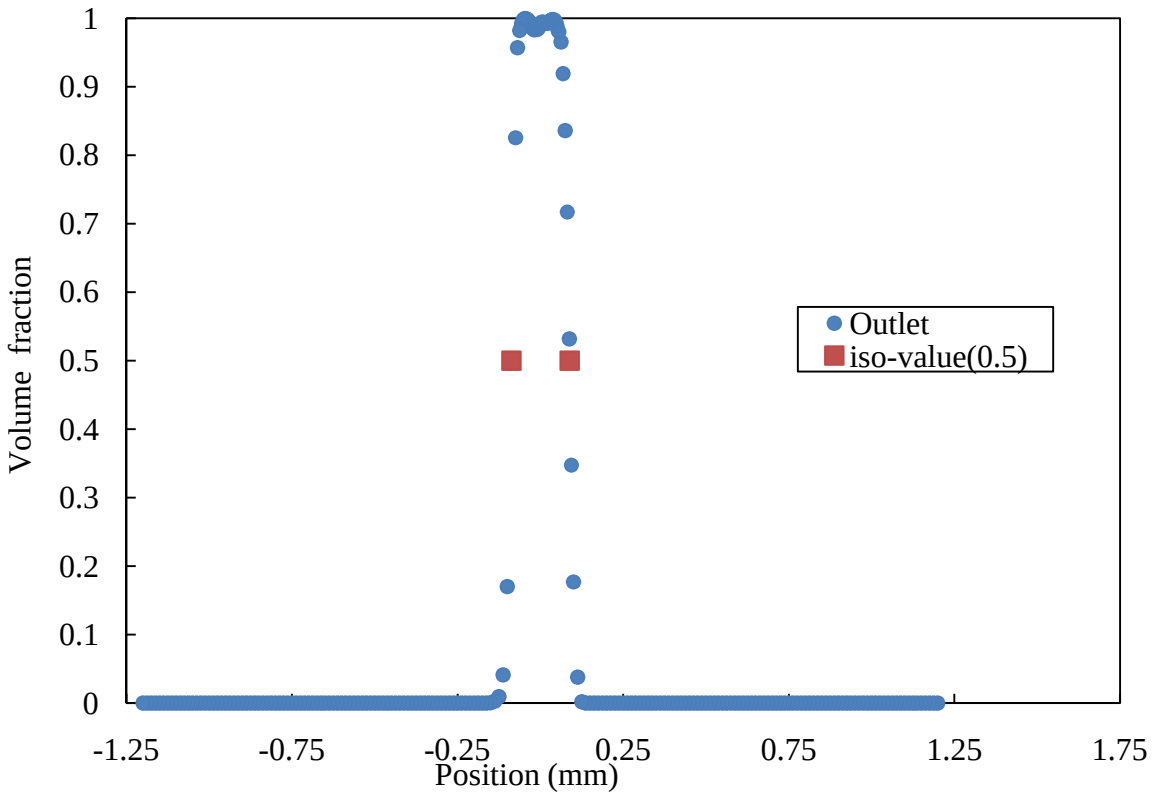

Figure 2.8 Variation of volume fraction of the sample flow along the transverse direction at the outlet for velocity ratio of 5.

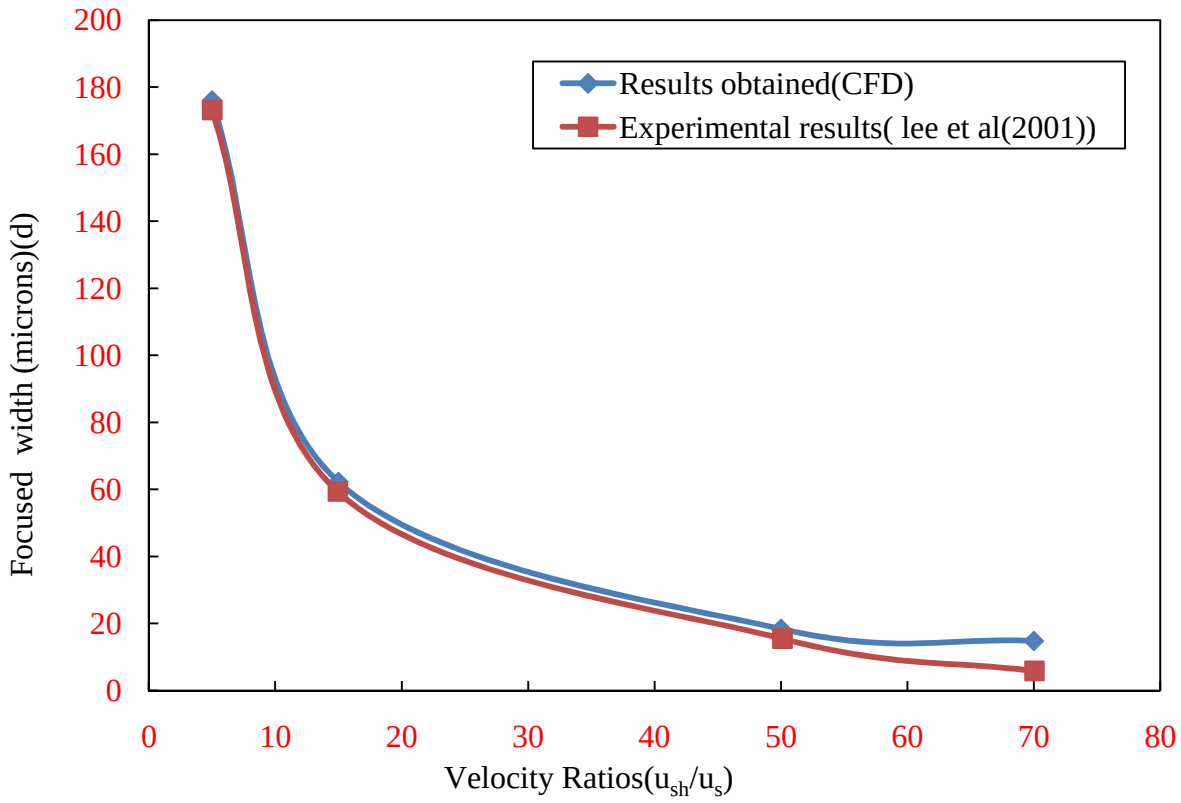

Figure 2.9 Comparison of focused width of the sample stream for different velocity ratios with the experimental results of Lee et al. (2001).

CHAPTER III

RESULTS AND DISCUSSION

The focusing width depends upon the geometry of the device and also assumed velocity profile of the flow. To investigate this, numerical simulations were performed by assuming the geometry as both 2-D and axisymmetric. The flow in both models was assumed to have a parabolic profile across the capillary width of D. This chapter also investigates the particle motion in the flow cytometer. Particles are tracked in the flow cytometer by using discrete phase model (DPM) of CFD code ANSYS FLUENT. Finally, the effect of the viscosity characteristics on the focusing width was studied by using non-Newtonian fluid in the simulation.

3.1 Analytical models

Hydrodynamic focusing (i.e. the narrowing of the sample flow) is caused by the sheath flow which is flowing around the sample. This is achieved by introducing sample flow at the center of the channel or the sheath stream. The cross-sectional dimension of the sample flow is predicted by using analytical models which can be derived from continuity equation. First 2-D and then axisymmetric flow geometries are chosen and the velocity in both cases is considered a parabolic profile in the capillary width of D.

The continuity equation is given by:

$$\nabla . \vec{v} = 0 \tag{3.1}$$

For 2-D focusing, the geometry along the direction perpendicular to the plane of the paper is considered as infinity. Assuming flow as fully developed laminar flow upstream of the nozzle the velocity flow profile in the capillary width D is parabolic with maximum velocity U_{max} at the center. As the sample and the sheath fluids have similar viscosities and the volume occupied by the sample fluid which was less than 0.5% compared to volume occupied by the sheath flow, the volume occupied by sample flow can be neglected. The theoretical ideal focusing width can be obtained by assuming 2D and axisymmetric cross-sectional geometry.

2D model:

The governing equation of steady, 2-d, Fully developed flow in the channel of width D is given by

$$\frac{d^2u}{dy^2} = \frac{1}{\mu}\left(\frac{dp}{dx}\right) \tag{3.2}$$

Where u is the velocity component along axis of the channel, $\left(\frac{dp}{dx}\right)$ is the pressure gradient which considered constant along the capillary.

The boundary conditions are:

$$\frac{du}{dy} = 0 \ @y = 0 \quad \text{(Symmetry)}, \qquad u = 0 \ @y = \pm\frac{D}{2} \quad \text{(No-slip)}$$

Exact solution by applying boundary conditions is given by;

$$U(y) = \frac{1}{2\mu}\left(\frac{dp}{dx}\right)\left(y^2 - \frac{D^2}{4}\right) \tag{3.3}$$

The maximum velocity in the channel is at the centerline and given by

$$U(y) = U_{max}\left(1 - \frac{4y^2}{D^2}\right) \tag{3.4}$$

The volumetric flow rate can be obtained by integrating above equation across the sample width D:

Volumetric flow rate for the sample fluid is given by:

$$Q_{sample} = \int_{\frac{-d}{2}}^{\frac{d}{2}} U_{max}\left(1 - \frac{4y^2}{D^2}\right)\,\mathrm{dy} = U_{max}.d\left(1 - \frac{1}{3}\left(\frac{d}{D}\right)^2\right) \tag{3.5}$$

$$Q_{Total} = Q_{sample} + Q_{sheath} = \frac{2}{3}Du_{max} \tag{3.6}$$

By solving Equations (3.5) and (3.6) hydrodynamic focusing ratio can be obtained

$$\frac{Q_{sample}}{Q_{Total}} = \frac{3}{2}\left(\frac{d}{D}\right)\left[1 - \frac{1}{3}\left(\frac{d}{D}\right)^2\right] \tag{3.7}$$

From above equation it can be seen that the focusing ratio is a non-linear function of the flow rate ratio. However, for small focusing ratios which are generally used in the flow cytometers, the equation has characters of a linear function.

Axisymmetric model:

The governing equations for a fully developed flow considering diameter of capillary D is given by

$$\frac{\mu}{r}\left(\frac{d}{dr}\left(r\frac{du}{dr}\right)\right) = \frac{dp}{dx} \tag{3.8}$$

By applying boundary conditions $\frac{du}{dr} = 0 \ @r = 0$ and u=0 $@r = \frac{D}{2}$and solving for the exact solution gives:

$$u(r) = \frac{D^2}{16\mu}\left(-\frac{\partial p}{\partial x}\right)\left(1 - \frac{4r^2}{D^2}\right) \tag{3.9}$$

The maximum velocity at the centerline and applying boundary condition

$u = u_{max} \ @r = 0$ gives

$$u(r) = u_{max}\left(1 - \frac{4r^2}{D^2}\right) \tag{3.10}$$

The sample flow rate is given by equation:

$$Q_{sample} = \int_0^{2\pi}\int_0^{\frac{d}{2}} u(r) r \, dr \, d\theta = \int_0^{2\pi}\int_0^{\frac{d}{2}} u_{max}\left(1 - \frac{4r^2}{D^2}\right) r \, dr \, d\theta \tag{3.11}$$

Similarly, solving total flow rate gives:

$$Q_{total} = u_{max}\frac{\pi d^2}{8} \tag{3.12}$$

Solving equations (3.11) and (3.12) for hydrodynamic focusing ratio

$$\frac{Q_{sample}}{Q_{Total}} = 2\left(\frac{d}{D}\right)^2\left[1 - \frac{1}{2}\left(\frac{d}{D}\right)^2\right] \tag{3.13}$$

The equations (3.7) and (3.13) show that hydrodynamic focusing ratio depends on the ratio of flow rate and cross-sectional geometry. Numerical simulations were carried out and the focusing ratios were obtained for both axisymmetric and 2D geometries.

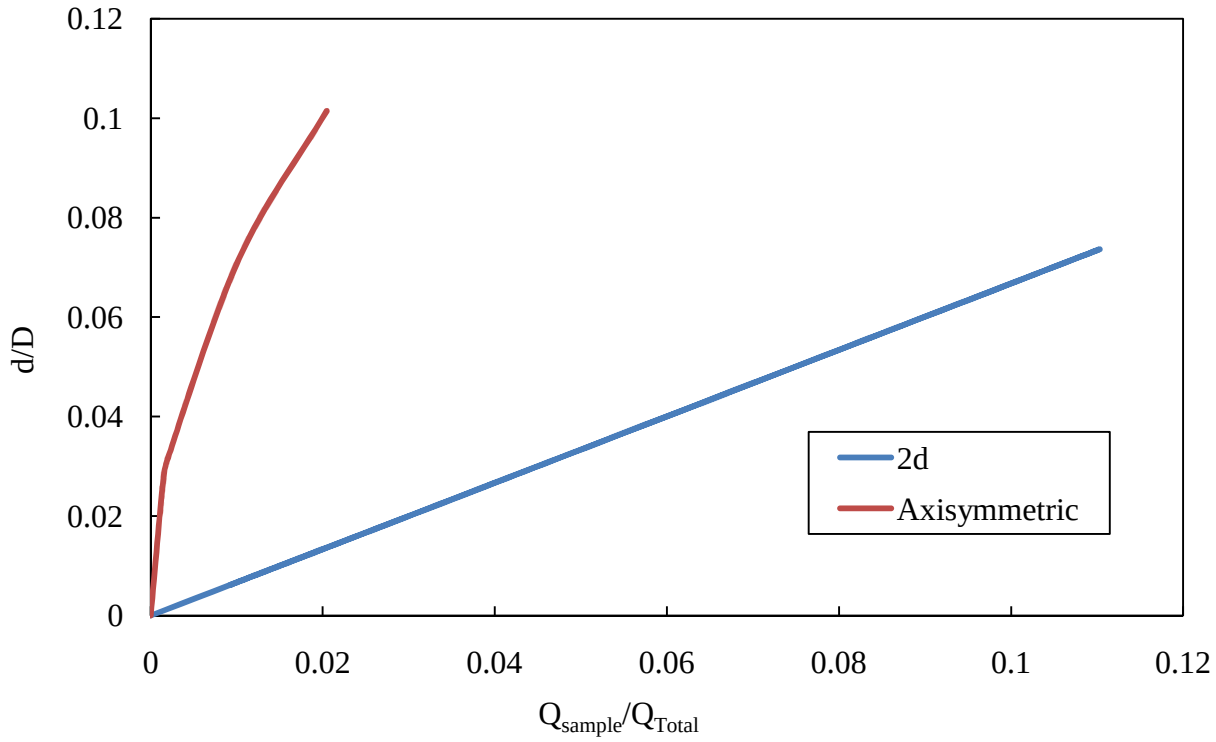

Figure 3.1 Focusing ratio$\left(\frac{d}{D}\right)$obtained from numerical solution as function of flow rate ratio for both 2-D and Axisymmetric model.

Figure 3.1 shows the plot of hydrodynamic focusing ratio obtained for velocity ratios 5, 15, 50 and 70 as a function of flow rate ratio.

3.2 Discrete Phase Model (DPM)

ANSYS FLUENT provides different models to study the multiphase flows. There are two approaches for the numerical calculation of multiphase flows, one Euler-Lagrange approach and Euler-Euler approach. The discrete phase model (DPM) available from ANSYS FLUENT follows Euler-Lagrange approach to track the particle. The fluid phase is considered as continuum phase by solving the Navier-stokes equations, while the dispersed phase is solved by tracking a large number of particles through the calculated flow field (Fluent, INC.). A main assumption made in the discrete phase model is that the dispersed phase occupies low volume fraction. The particle trajectories are computed individually at specified intervals during the fluid phase calculation. This model can be used to solve or model spray dryers, fuel combustion and particle-laden flows. This model is appropriate to for the modeling of problems where the volume fraction of the second phase is neglected but inappropriate where the second phase volume fraction is not neglected.

3.3 Equations of motion of particles

The particle balance equation of particle is integrated to predict the trajectory of the discrete phase model. The force balance equates the particle inertia with the forces acting on the particle and is given by:

$$\frac{du_p}{dt} = F_D\left(u - u_p\right) + \frac{g_x(\rho_p - \rho)}{\rho_p} + F_x \qquad (3.13)$$

Where $F_x$is an additional acceleration (force/unit particle mass) term,$F_D\left(u-u_p\right)$ is the drag force per unit particle mass.

Drag force F_D is given by

$$F_D = \frac{18\mu}{\rho_p {d_p}^2}\frac{C_D Re}{24} \tag{3.14}$$

Where u is the fluid phase velocity, u_p is the particle velocity, μ is the molecular viscosity of the fluid, ρ is the fluid density, ρ_p is the density of the particle, and $d_p$is the particle diameter, Re is the relative Reynolds number given as :

$$Re = \frac{\rho\, d_p|u_p-u|}{\mu} \tag{3.15}$$

Additional forces(F_x) which can be included in the equation 3.1 are virtual mass force, forces in rotating frame of references, thermo-phoretic forces, Brownian forces and Saffman's lift forces.

The trajectory equations and other equations involving heat and mass transfer to and from the particle are solved by stepwise integrating over discrete time steps. ANSYS Fluent discrete phase model provides different laws for drag coefficients C_D like spherical drag law, non-spherical drag law, and Stokes-Cunningham drag law. The non-spherical drag law uses shape factor φ which is defined as ratio of surface area of sphere having the same volume as the particle to the actual surface area of the particle to model the particles which have shapes other than the sphere.

3.4 Particle tracking

Particles are introduced into the microfluidic device and their motion is tracked using discrete phase model (DPM) by ANSYS FLUENT. The trajectory of the particle is studied or observed by injecting particle at the inlet of the center channel. The particles are introduced along with the sample and their motion is studied. As the function of a microflow cytometer is to study the properties of the cells which flow in a single file along the region of interrogation, the hydrodynamic focusing phenomena is observed by tracking the particle and investigating if the particle is focused enough so that they flow one by one along the focusing region. The behavior of the particle and motion of the particle on the along the device is studied.

Numerical simulations were carried out by injecting particles into the center channel along with the sample flow. ANSYS FLUENT provides discrete phase model (DPM) which allows us to simulate a discrete second phase in a Lagrangian frame of reference. The second discrete phase consist of the particles dispersed in the continuous phase and ANSYS FLUENT computes the trajectories of these discrete phase particle with the option of calculating heat and mass transfer to/from them. First the steady solution is obtained by solving the continuous phase. After that the discrete phase is included in the model by defining the initial position, velocity and size of the particles.

The discrete phase model is enabled and the interaction with the continuous phase option is also enabled. The particles are treated in a transient fashion to find the trajectory of the particle. ANSYS FLUENT provides different drag laws to specify tracking parameters of the discrete phase. The spherical drag law is chosen and the Saffman lift force is chosen for the physical model. The initial condition for the discrete phase is set

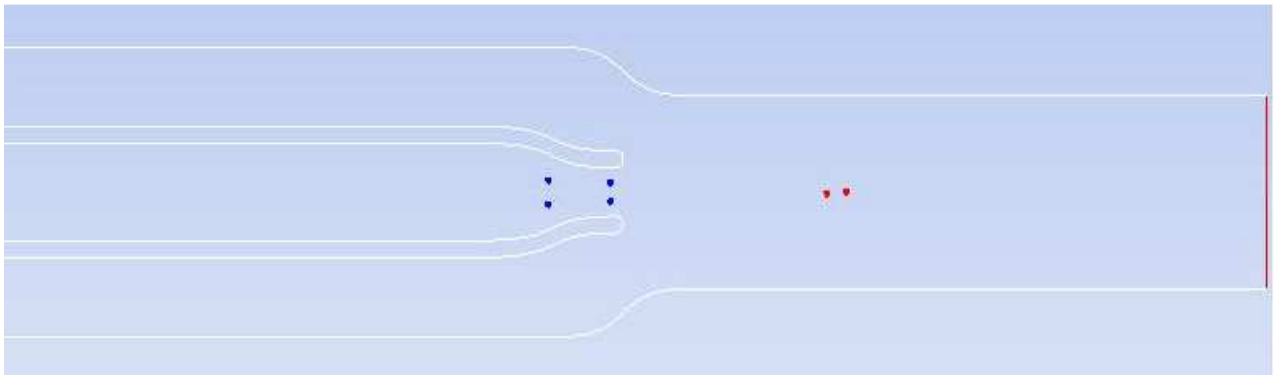

Figure 3.2 Numerical trace results of microparticle of diameter 6 microns in X-Y plane.

by introducing injections. ANSYS FLUENT provides 11 types of injections which include single, group, cone, surface etc. To observe if the particles are focused i.e. move in single file at the detection region, two particles are injected at the inlet of the center channel into sample flow at same the time. The properties of particles are set and diameter chosen was 6 microns which is size of typical red blood cell. Then the trajectories of two particles are simulated over time as they flow along with the sample fluid downstream. Figure 3.2 shows the simulated trace results of six particles injected at the inlet with differences of time 20 sec among them. As they are injected from same points and they are identical they tend to follow same path. We can see the particle placed on top of one another when they flow through the inner channel and as they exit the channel they are affected by the sheath flow. As they move downstream further they are focused and flow in a single file through the device, where they can be detected individually. Thus they flow through focused region maintaining distance between them and in a sequential manner. The trajectory of the particles with diameters 6, 12, 48 µm with velocity ratio of 5 in the microfluidic device was also observed for same time step and can be seen in the figure 3.4. It can be seen that the particles with diameter 6 µm stay longer time in the device than others. The particles can be introduced at any point in the center channel and it can be observed that all the particles are focused as they exit the nozzle and move downstream along the capillary.

Particle trajectories and their velocities can be plotted once the solution is obtained. Figure 3.3 shows the position of a single particle on X-Y plane along the channel. Here the particle is injected from a distance of 0.3mm from the center along positive Y-axis. As the particle approaches the exit of the inner nozzle, it is affected by

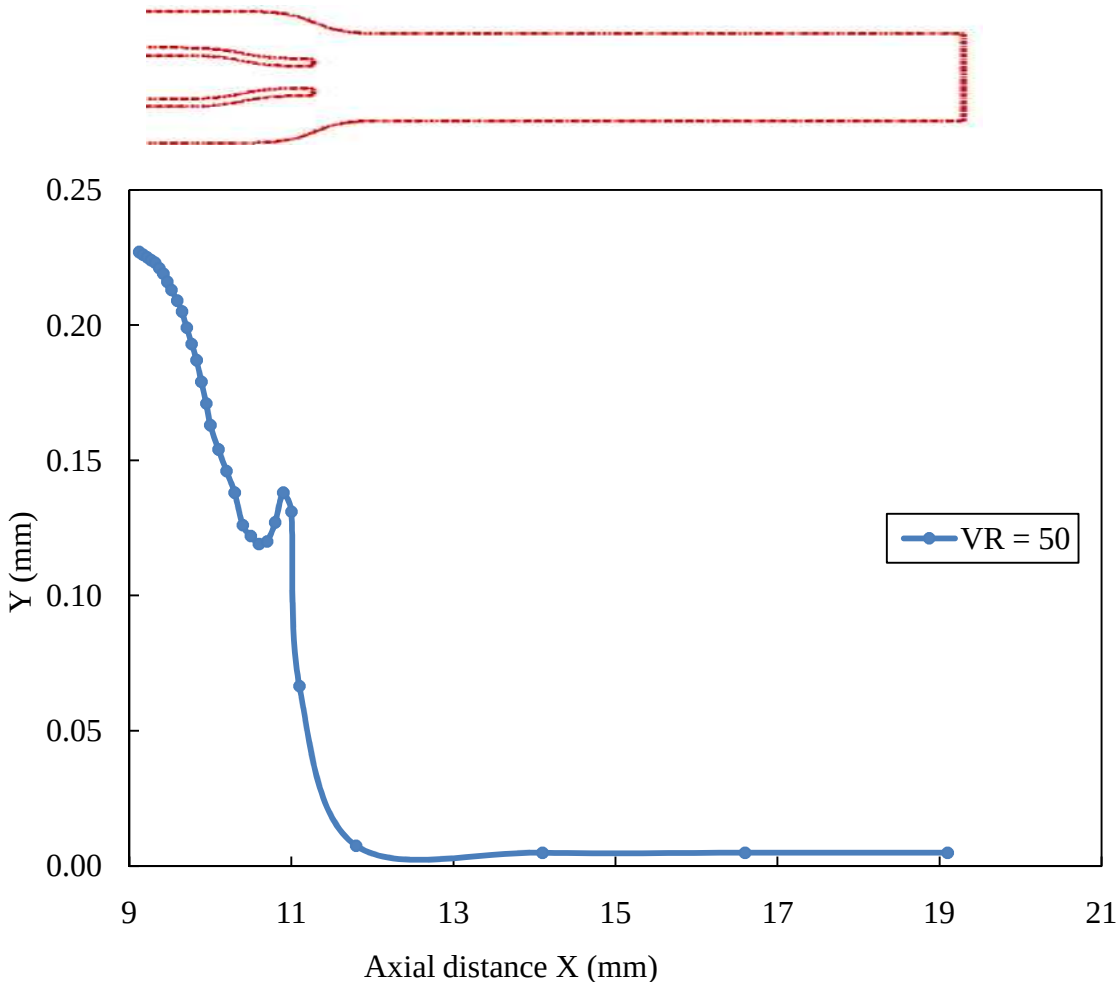

Figure 3.3 Particle position along the channel in X-Y plane for velocity ratio (u_{sh}/u_s) of 50.

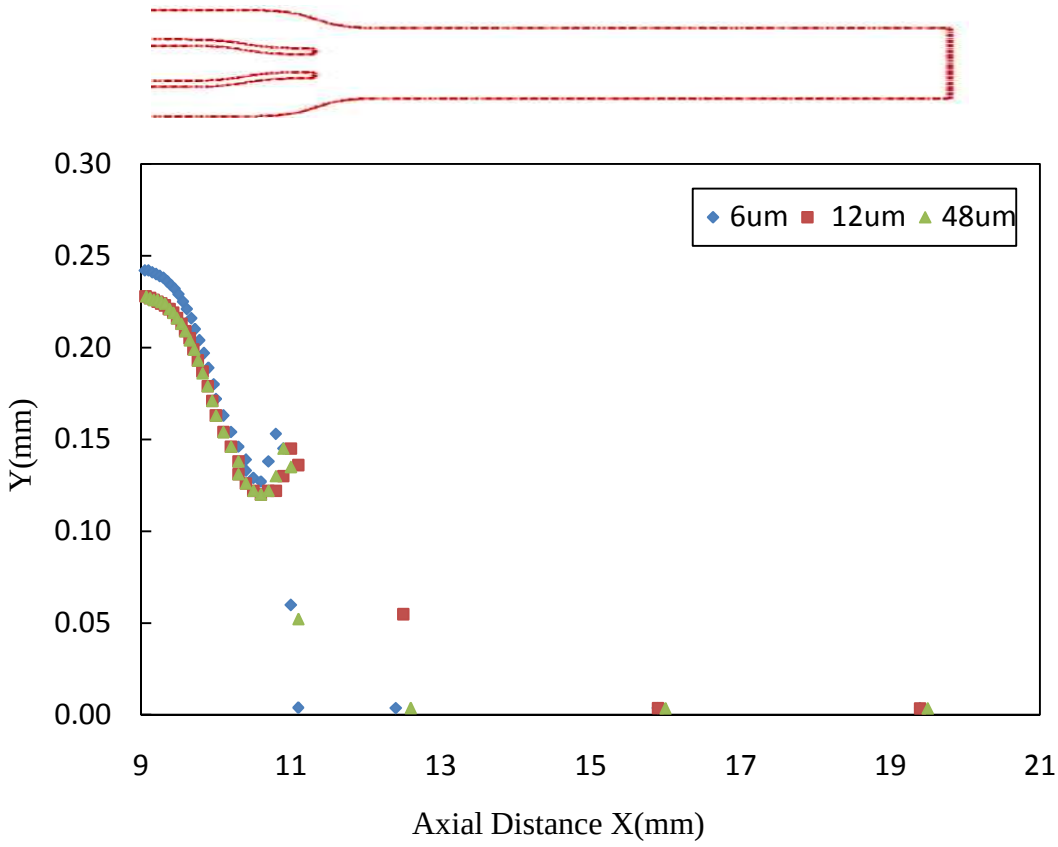

Figure 3.4 Trajectory of the particles in X-Y plane for velocity ratio of 50 for particle diameters of 6, 12, 48 µm.

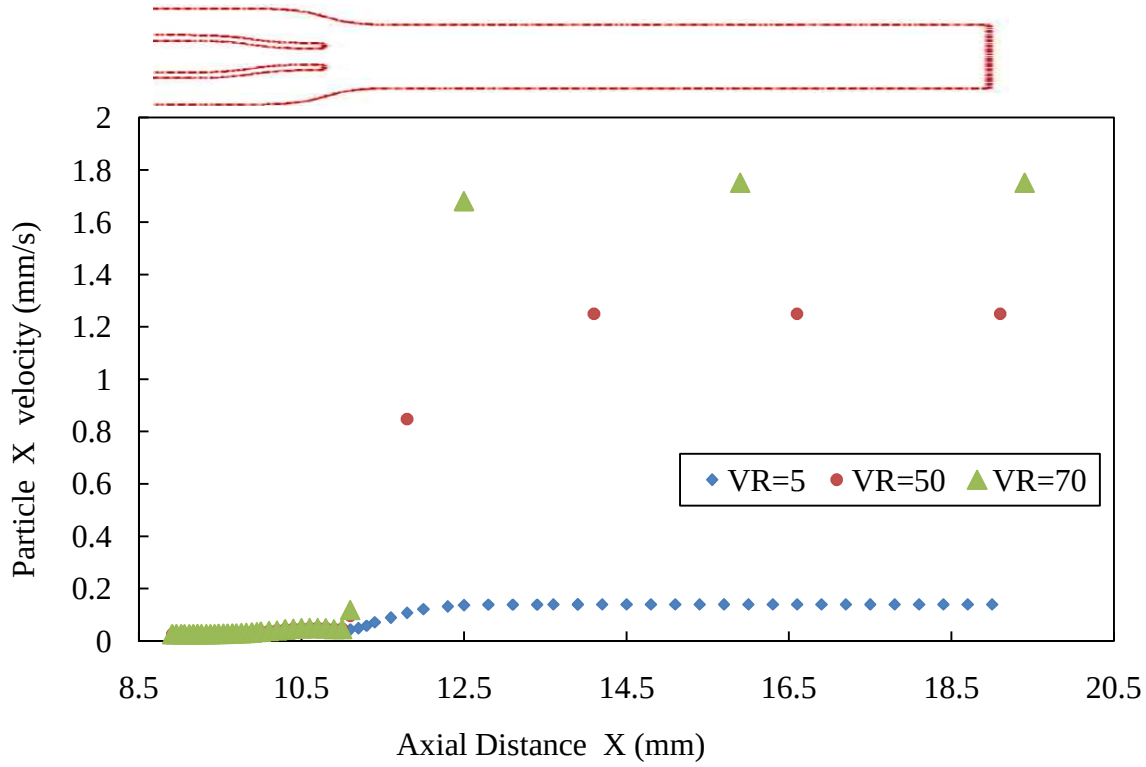

Figure 3.5 Particle velocity variations across the channel velocity ratios (u_{sh}/u_s=5, 50, 70).

higher velocity of the sheath flow and tends to move towards the center line of the channel, thus exhibiting hydrodynamic focusing.

3.5 Effect of viscosity

Simulations were performed to study the effect of the sample fluid properties on the focusing phenomena. Sample fluid which was used above was replaced with the fluid similar to human blood and the physical properties are defined. The density of the blood given was 1060 Kg/m^3. Blood sample was considered as non-Newtonian and viscosity is modeled using Carreau-Yasuda model. A User Defined Function (UDF) was written to specify the viscosity of the sample blood fluid (Appendix B).

ANSYS FLUENT provides few models like Power law, Cross model, Herschely-Bulkley for modeling non-Newtonian flows. For incompressible Newtonian flows shear stress is proportional to rate of deformation tensor $\overline{D}$ and is given by:

$$\overline{\tau} = \mu\overline{D} \tag{3.11}$$

Where

$$\overline{D} = \left(\frac{\partial U_j}{\partial X_i} + \frac{\partial U_i}{\partial X_j}\right) \tag{3.12}$$

For some Non-Newtonian Fluids the shear stress is written as in terms of non-Newtonian Viscosity η:

$$\overline{\tau} = \eta\left(\overline{D}\right)\overline{D} \tag{3.13}$$

In non-Newtonian models available in FLUENT, η is considered as function of shear rate $\dot{\gamma}$ only and is related to second variant of $\overline{D}$ and give as:

$$\gamma \coloneqq \sqrt{\overline{D} : \overline{D}} \tag{3.14}$$

Carreau-Yasuda Model is given by the equation:

$$\frac{\eta - \eta_\infty}{\eta_0 - \eta_\infty} = \left(1 + (\lambda\dot{\gamma})^a\right)^{(n-1)/a} \tag{3.15}$$

Where, η_0= Viscosity at zero shear rate, η_∞= Viscosity at infinite shear rate, λ = Time relaxation constant, n = exponential index, a= model constant.

The physical properties used to model the blood as Carreau-Yasuda model (Cho and Kensey, 1991) are given in the table 3.1.

After the solution is obtained, the focusing width is obtained and plotted against velocity ratios of sheath and sample. This may be due to the reason that the sample blood flow from center channel has lesser flow rate when compared to sheath fluid thus influencing the focusing phenomena. The velocity profiles of both the blood and water sample can be seen in the Figure 3.6. The plot shows that due to the viscosity effect, the maximum velocity for the blood-like fluid is less than the water sample, thus slightly influencing the focusing behavior of the blood sample. Figure 3.7 shows the effect of sample fluid properties on the focusing width for both water and blood as sample flow. From the graph we can see the focusing widths are fairly close to the each other with greatest difference of 20% at the velocity ratio of 15. Mass flux at the inlet and the outlet was checked. Percentage difference in the mass flux was calculated at the inlet and the outlet and a value of -4.22108E-06 was recorded for the velocity ratio of 5. As the value obtained is very low we can conclude that the mass is conserved.

η_0 (P)	η_∞(P)	a	n	λ(s)
0.56	0.00345	2	0.3568	3.313

Table 3.1 Carreau model parameters of non-Newtonian blood (Cho and Kensey, 1991).

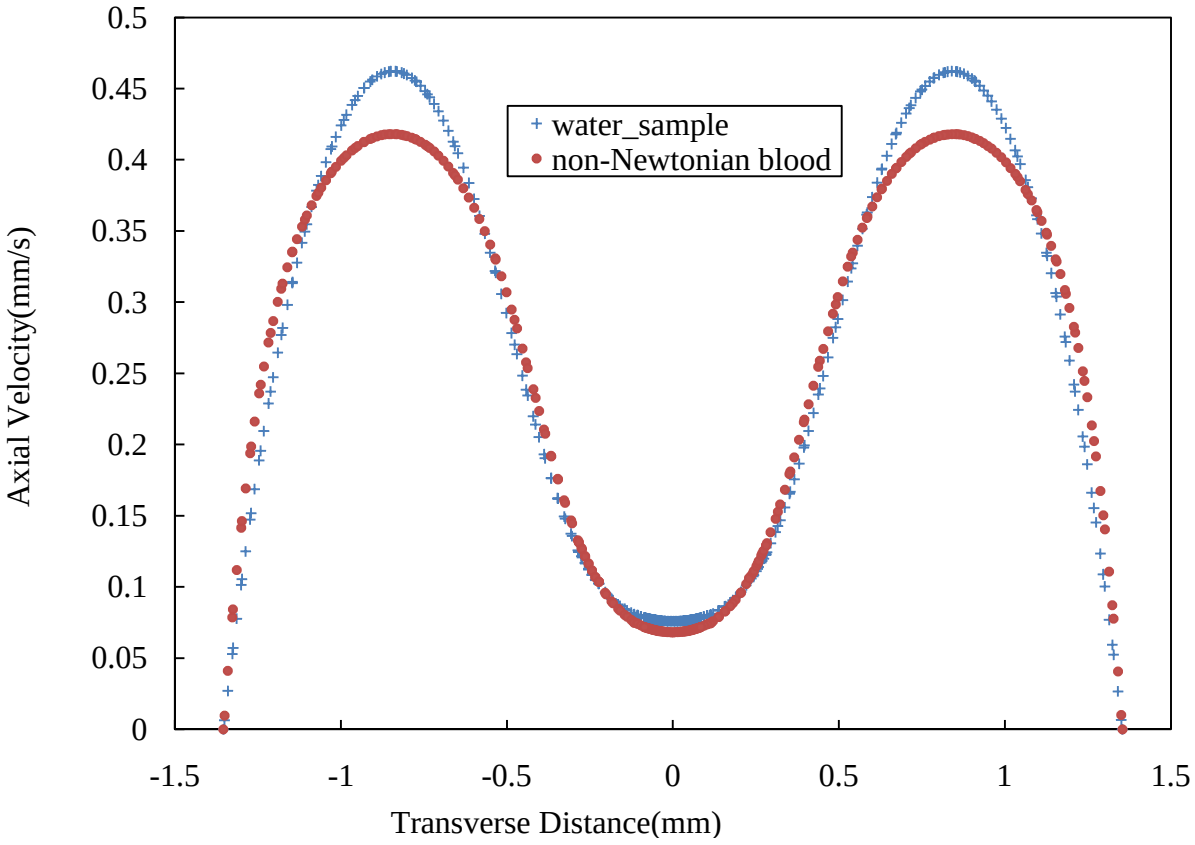

Figure 3.6 Transverse distribution of axial velocity at the location of 11.2 mm and velocity ratio of 15 for both water and non-Newtonian blood sample.

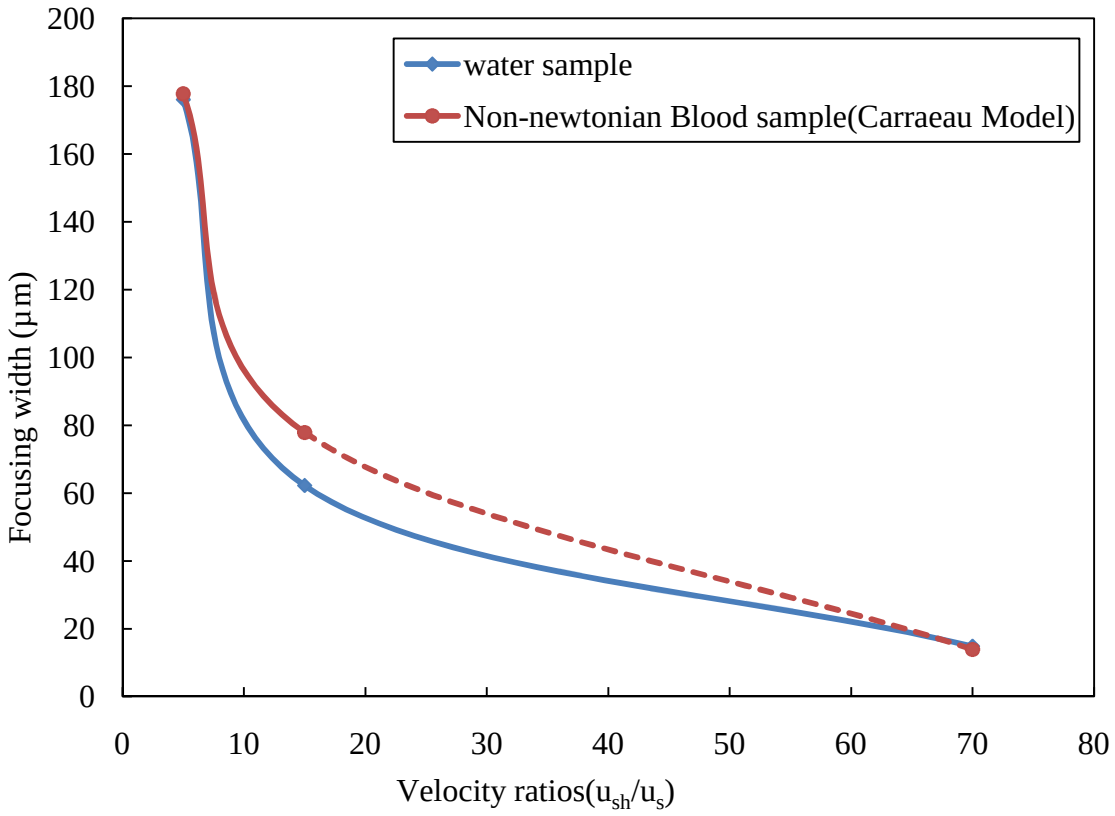

Figure 3.7 Effect of sample fluid properties on focused width at different velocity ratio (u_{sh}/u_s).

Chapter IV

CONCLUSIONS AND RECOMMENDATION

4.1 Summary

In this work, hydrodynamic focusing behavior in a microflow cytometer was studied. Numerical simulations were performed to study the 2-D hydrodynamic focusing phenomena in a microflow cytometer fabricated by Lee et al. (2000). The geometry was modeled using ICEM CFD meshing software from ANSYS with a grid size of 892k cells. Finer cells were placed at the convergent part of the nozzle to resolve the sudden variations in the flow properties. A hydrodynamic focusing phenomenon was studied by varying the velocities of both sample and sheath flows flowing through the center and outer channels respectively of the microflow cytometer. Both the sample and the sheath flows were treated as 2-D, laminar, incompressible and isothermal and the no-slip condition was used at the walls of the microfluidic device .The velocity ratios (velocity of sheath to sample flow ratio) were varied from 5 to 70 and the change in the focusing width with the velocity ratios was investigated. The Volume of Fluid model (VOF) provided by ANSYS FLUENT was used to model the interaction between the sheath and the sample flows. The Discrete Phase Model (DPM) of ANSYS FLUENT was used to inject the particles with the sample flow and track their motion. Numerical simulations were carried out with the particles injected into the sample flow with defined diameter and density and were tacked to check if the particles are focused. The results confirm the

hydrodynamic focusing of the sample flow and as the particles moved in a single file in the horizontal X-Y plane towards the detection region. The effect of the particle diameter on the focusing behavior was also studied. In addition, the effect of the viscosity on the focusing width was studied by introducing different Newtonian and non-Newtonian fluids into the micofluidic device. Simulations were performed by considering blood as non-Newtonian sample fluid whose viscosity was modeled by Carreau-Yasuda model. A User Defined Function (UDF) was implemented to define the viscosity of the blood in ANSYS FLUENT.

4.2 Conclusions

First the effect of velocities of both the sheath and the sample flow on focusing width was explored. From the calculated results the predicted focusing width tends to decrease with the increase in the velocity ratio as the high velocity sheath flow squeezes the sample fluid which is having a lower velocity. The focusing width less than 10 µm was achieved by increasing the velocity ratio to 70. The predicted results match well with the experimental results of Lee et al. (2001) with errors of 1.6% and 4.8%for velocity ratios of 5 and 15 respectively.

Particles of size 6 µm (typical of the size of red blood cells) were injected into the sample flow. The particles were injected from different locations chosen arbitrarily and were tracked using the discrete phase model (DPM) available from ANSYS FLUENT. The trajectories of the particles were obtained after the simulations were performed. As the particles move downstream they are focused and flow in a single file through the device after they exit the inlet nozzle, where they can be studied individually. Thus they

flow through the focused region maintaining the distance between them and in a sequential manner.

To study the effect of the fluid properties on the focusing width, non-Newtonian model of blood was used and the simulations were carried. The blood flow was modeled using Carreau-Yasuda model and a user defined function (UDF) was used to model the viscosity in ANSYS FLUENT. The focusing widths were calculated for velocity ratios(u_{sh}/u_s) of 5, 15, 70 and the results revealed only minor deviation from those with water as the sample fluid.

4.3 Suggestions for future work

The present study was done to explore the 2-D hydrodynamic focusing phenomenon in a microflow cytometer. The model can be developed so that sample flow can be focused in 3-D and by improving the geometry, the functioning of a cytometer can be improved.

Hydrodynamic focusing eliminates the use of small nozzles which may cause clogging in case of polymer solutions or large particles. Modeling complex polymer solutions used for electrospinning of nanofibers and the effect of the hydrodynamic forces on particles like DNA, sperm, carbon-nanotubes and their flow behavior through the channels can be studied.

BIBILIOGRAPHY

1. Choi. S and Park. J.K, "Continuous hydrophoretic separation and sizing of microparticles using slanted obstacles in a microchannel", Lab on a Chip**7** (7), 2007, pp.890-897.

2. Lee. G.-B, Hung. C.I, Ke. B.J, Huang, G.R, Hwei.B.H, and Lai.H.F, "Hydrodynamic Focusing for a Micromachined Flow Cytometer", Journal of Fluids Engineering,123 (3),2001: pp.672-679.

3. Lin. C.H, Lee. G.B, Fu. L.M, Hwey. B.H, "Vertical focusing device utilizing dielectrophoretic force and its application on microflow cytometer." Microelectromechanical Systems, 13 (6), 2004, pp.923-932.

4. Mao. X, Waldeisen. J, Haung .T.J, " Microfluidic drifting"-implementing three-dimensional hydrodynamic focusing with a single-layer planar microfluidic device." Lab on a Chip**7** (10), 2007, 1260.

5. Simonnet. C and Groisman. A," High-Throughput and High-Resolution Flow Cytometry in Molded Microfluidic Devices", Analytical Chemistry, 78 (16):2006 pp.5653-5663.

6. Tsai. C.H, Hou. H.H, Fu. L.M, "An optimal three-dimensional focusing technique for micro-flow cytometers." Microfluidics and Nanofluidics**5** (6): 2008, pp.827-836.

7. Walker. G.M and Beebe. D.J, "A passive pumping method for microfluidic devices." Lab on a Chip2 (3): 2002, pp.131-134.

8. Xuan. X and Li. D, "Focused electrophoretic motion and selected electrokinetic dispensing of particles and cells in cross-microchannels.", Electrophoresis26 (18):2005, pp.3552-3560.

9. Srivastva. Y, Rhodes. C, Marquez. M and Thorsen, T, "Electrospinning hollow and core/sheath nanofibers using hydrodynamic fluid focusing", Microfluid nanofluid (5):2008, pp.455-458.

10. Taylor.G.I. "Electrically driven jets" Proc R Soc London, Ser A ,1969; 313:pp.453

11. Thangawng. A. L, Howell Jr. P.B., Richards. J. J, Erickson. J.S and Ligler. F.S, “A simple sheath-flow microfluidic device for micro/nanomanufacturing: fabrication of hydrodynamically shaped polymer fibers”, Lab Chip, 2009, (9), pp.3126–3130.

12. Lee. M.G., Choi. S and Park. J.K, “Three-dimensional hydrodynamic focusing with a single sheath flow in a single layer microfluidic device”, Lab chip, 2009, pp.3155-3160.

13. Yang. A.S and Hseih. W.H, “Hydrodynamic focusing investigation in a micro-flow cytometer”, Biomed Micro devices (9): 2007, pp.113-112.

14. Hirt. C. W and Nichols. B. D,"Volume of Fluid (VOF) Method for the Dynamics of Free Boundaries", Journal of Computational Physics, (39), 1981,pp. 201-225.

15. Lee. M.G, Choi. S and Park. J, “Inertial separation in a contraction-expansion array microchannel", Journal of chromotography A, 2010, in press.

16. Cho. Y.I and Kensey. K.R, "Effect of non-Newtonian viscosity of blood on flows ina arterial vessel.", Biorheology, 1991; 28(3-4):pp.241-62.

17. Jacobson .S.C, Ramsey. J.M ," Electrokinetic Focusing in Microfabricated Channel Structures ", Anal Chem (69):,1997,pp.3212–3217.

18. FLUENT, User’s Guide, Fluent Inc., Lebanon, USA ,2009

19. Morel.T, " Comprehensive design of Axistmmetric wind tunnel contractions", Journal of Fluids Engineering (97):1975, pp.225-233.

Appendix A

User defined function (UDF) used to define viscosity of non-Newtonian fluid.

```
#include ”udf.h”

DEFINE_PROPERTY(carreau_viscosity,c,t)

{
 real mu_carr, gamma,mu_inf,rho,mu0, n,K ;
 mu_inf 0.00345
 rho=1050
 mu0=0.056
 n=0.3568
 K=3.133

real mu_carr, gamma;
real n1 =(n-1)/2;

gamma = C_STRAIN_RATE_MAG(c,t);
mu_carr = mu_inf +(mu0 - mu_inf)*pow((1+pow(K,2)*pow(gamma,2)), n1 );
return mu_carr;
}
```

VITA

Samuel Ariekela

Candidate for the Degree of

Master of Science

Thesis: NUMERICAL INVESTIGATION OF THE HYDRODYNAMIC FOCUSING PHENOMENA IN A MICROFLOW CYTOMETER

Major Field: Mechanical and Aerospace Engineering

Biographical:

Personal Data: Born in Hyderabad, India, May 27th

Education:

Completed the requirements for the Master of Science in Mechanical and Aerospace Engineering at Oklahoma State University, Stillwater, Oklahoma in May 2011.

Completed the requirements for the Bachelor of Engineering in Mechanical Engineering at Chaitanya Bharathi Institute of Technology, Osmania University, Hyderabad, India in 2007.

Experience:

Worked as a production engineer for Balaji Structural Engineers and Fabricators, Hyderabad, India (June 2007 – July 2008).

Graduate Teaching Assistant for Mechanical and Aerospace Engineering, Oklahoma State University, OK, USA (January 2010 – May 2011).

Research experience in the field of Computational Fluid Dynamics (CFD) under guidance of Dr. Khaled A.Sallam at Oklahoma State University, OK, USA.(August 2009 – May 2011).

Name: Samuel Ariekela Date of Degree: May, 2011

Institution: Oklahoma State University Location: Stillwater, Oklahoma

Title of Study: NUMERICAL INVESTIGATION OF THE HYDRODYNAMIC FOCUSING PHENOMENA IN A MICROFLOW CYTOMETER

Pages in Study: 60 Candidate for the Degree of Master of Science

Major Field: Mechanical and Aerospace Engineering

Scope and Method of Study:

Simulations were performed to study the 2-D hydrodynamic focusing phenomena in a microflow cytometer. The hydrodynamic focusing phenomenon was studied by varying the velocities of both the sample and the sheath flows flowing through the center and the outer channel of a microflow cytometer. The geometries studied include both 2D and axisymmetric ones. Velocity ratios (velocity of sheath to sample flow ratio) were varied from 5 to 70 and the results include the change in the focusing width. Discrete phase model (DPM) of ANSYS FLUENT was used to inject particles with different sizes along the sample flow and their trajectories were tracked. The focusing characteristic of non-Newtonian fluids in comparison with Newtonian fluids was also studied.

Findings and Conclusions:

The predicted focusing widths tend to decrease with the increase in the velocity ratio. A focusing width less than 10 µm can be achieved by increasing the velocity ratio to 70. It is also observed that the focusing ratio is the function of flow rate ratio and depends on the geometry of the sample flow. The trajectory of the particles in the cytometer is tracked and the results confirm the hydrodynamic focusing of the sample flow as the particles moved in a single file in the horizontal X-Y plane toward the detection region. The focusing width was calculated for velocity ratios (u_{sh}/u_s) of 5, 15, and 70 for both non-Newtonian and Newtonian fluids and the results revealed only slight deviation in the focusing widths.

ADVISOR'S APPROVAL: Khaled A. Sallam